**ORIGINAL PAPER**

# Analysis of Fracture Evolution Characteristics and Formation Mechanism of Inter-Layer Rock Under Different Mining Areas

Jie Zhang[1,2] · Jianjun Wu[1,2] · Tao Yang[1,2] · Sen Yang[1,2] · Yifeng He[1] · Shoushi Gao[1] · Bing Peng[3]

## Abstract

As the shallow coal seams are gradually being exhausted, mining of the lower group of coal seams in the shallowly buried proximity coal seam group becomes inevitable. Due to geological conditions affecting the upper group coal seams, various coal mining methods have resulted in a significant number of non-sufficient and sufficient collapse mining areas. The presence of water and gas in these mining areas can potentially impact the safe production of the lower group coal seams through inter-layer rock fractures. Therefore, studying the evolution characteristics and formation mechanism of inter-layer rock fractures is of utmost importance. In this paper, we employ theoretical analysis, numerical simulation, and similar simulation methods to investigate the evolution characteristics and formation mechanism of inter-layer rock fractures during the mining of the lower $3^{-1}$ coal seam. We specifically focus on the formation of different mining areas in the upper $2^{-2}$ coal seam, using the mining of $2^{-2}$ and $3^{-1}$ coal seams in the Hanjiawan coal mine as our research context. The study results reveal that the inter-layer rock fractures exhibit an overall positive trapezoidal distribution in different mining areas. We quantify the variation in density and width of inter-layer rock fractures in the two mining areas by utilizing the concept of rock damage degree. We analyze the overall damage degree, tensile damage degree, and shear damage degree ratios. The formation of inter-layer rock fractures is primarily influenced by the combined effect of various coal mining methods in both the upper and lower coal seams. The stress changes resulting from mining activities in these seams contribute to the development of transverse separation fractures and longitudinal breaking fractures within the inter-layer rock. The stress changes induced by mining operations in the upper and lower coal seams have been analyzed, and distinct stress regions have been identified. To understand the mechanism of inter-layered rock fracture development in the upper and lower coal seams, a mechanical expansion model of inter-layer rock fractures has been constructed for different stress regions.

## Highlights

- The evolution process and development characteristics of inter-layered rock fractures, as well as their differences when different coal mining methods are employed in the upper coal seam, have been revealed.
- To determine the influencing factors and development patterns of inter-layered rock fractures under different coal mining methods.
- Quantitatively comparing and analyzing the damage of inter-layered rock and the percentage of damage degree under different coal mining methods, we found that the damage degree was 61% and 52%, respectively.
- The study shows that when mining the upper coal seam, the inter-layer rock primarily extends through primary microscopic fractures. On the other hand, when opening the lower coal seam, the main development is observed in macroscopic tension fractures and shear misalignment fractures.
- Based on the study of the development process of macroscopic fractures and microscopic fractures in the inter-layered rock, the mechanism of fracture development and evolution of the inter-layered rock under different coal mining methods has been determined.

✉ Jianjun Wu
   wjj910928@126.com

1   School of Energy Engineering, Xi'an University of Science and Technology, Xi'an 710054, China

2   Key Laboratory for Mining and Disaster Prevention in the West of the Ministry of Education, Xi'an 710054, China

3   Shaanxi Mineral Resources Investigation and Evaluation Center, Xi'an 710054, China
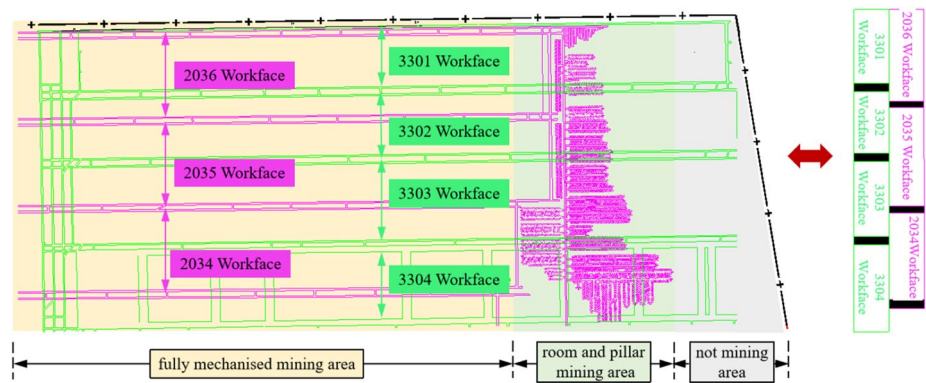
## 1 Introduction

The ShenFu coalfield is typically characteristics by geological deposits in close proximity to the buried shallow seams. Due to these geological deposit conditions, different mining methods are used for the upper seam (Zhu et al. 2018; Zhu 2018; Huang and Han 2019). To improve the mining rate of the upper coal seam and increase economic efficiency, a combination of room and pillar coal mining methods and long-wall fully mechanized coal mining methods are commonly employed. However, the different mining areas formed by the upper coal seam mining have a significant impact on the inter-layer rock structure and fracture development. The fracture channels formed by these mining methods make the lower coal seam vulnerable to water collapse, spontaneous combustion of the remaining coal seam, and gas leakage. These factors pose a great threat to the life and safety of underground personnel and create safety hazards for the mine's production (Yu et al. 2018; Zhang et al. 2017).

At present, a lot of research has been done on the transport of overburden structure and the law of mine pressure on both upper and lower coal seams of shallowly buried close coal seams using the long-wall fully mechanized coal mining method (Huang et al. 2018; Wang et al. 2016; Zhu et al. 2019; Xu et al. 2020). However, the research on the evolution process, distribution characteristics, and formation mechanism of rock fractures between the upper and lower coal seam mining layers is not comprehensive enough. Regarding the fracture development mechanism of the overlying rock seam, the mechanism of secondary expansion of fractures in the overlying rock seam at the mining site during the downward mining of the shallowly buried proximity coal seam group was studied, and the fracture expansion direction, fracture initiation stress intensity factor, expansion rate, and fracture development height calculation formulae were determined (Huang et al. 2019; Yang and Wang 2018). The study focused on the dynamic distribution and evolution law of fractures in the bottom slab under different stresses caused by mining. The mechanical mechanism of fracture opening and expansion in different region was determined (Zhang et al. 2015). In addition, numerical calculations and simulation were used to study the evolution of overburden fractures and air leakage channels in shallowly buried coal seams subjected to repeated mining. The study also investigated the development of porosity in overburden fractures and the height of fracture development at different stages (He et al. 2020). Furthermore, the study examined the degree of fracture penetration in tensile damage strata,

revealing that when the compressive stress exceeds the compressive strength, longitudinal fractures caused by tensile damage will penetrate the laminate strata (Lu et al. 2020). Based on the key layer theory, an analysis was conducted on the height of fracture development in the overlying rock layer. This analysis led to the determination of judgement criteria and the ground fracture development pattern (Zhang et al. 2021). As the research progressed, quantitative description and fractal dimension analysis of overlying rock fractures were performed (Wang 2022). In addition, the geological endowment conditions of thin bedrock at shallow burial depths in the ShenFu mine were considered. The study focused on the expansion law, distribution characteristics, and key layer relationships of surface hydraulic conductivity fractures and gas transport fractures. Furthermore, mechanical models were constructed to understand the structural breakage of these fractures with inter-layered rock layers (Zhu et al. 2020; Liu et al. 2021; Cai et al. 2022; Feng et al. 2021). However, most of the previous studies have primarily focused on the overall fracture changes in the overburden rock under a single coal mining method. The research on the evolution law, distribution characteristics, and formation mechanism of inter-layered rock fractures under different mining areas is incomplete. In contrast, foreign scholars have mainly focused on the expansion of microscopic fractures in the rock seam, studying evolutionary laws and stress inter-relationships (Song et al. 2023; Wang et al. 2019, 2021). Their research tends to be more focused on the rock body and microscopic level, and the research methods mostly involve laboratory studies and numerical simulation calculations (Aben et al. 2016; Gong et al. 2023).

After mining of the $2^{-2}$ coal seam in HanJiaWan coal mine, three different areas were formed: the not mining area, the room and pillar-mining area, and the fully mechanized mining area. Due to the different coal mining methods in the upper coal seam, there are significant differences in the stresses on the inter-layer rock. As a result, the fracture evolution, expansion pattern, and formation mechanism of the inter-layer rock during the mining of the lower $3^{-1}$ coal seam exhibit different states. The unclear nature of fracture development poses a potential threat to mine safety and production. Therefore, this study focuses on the inter-layer rock between the $2^{-2}$ and $3^{-1}$ coal seams in HanJiaWan coal mine. It aims to investigates the distribution characteristics and formation mechanism of inter-layer rock under different mining areas during the mining process of the upper and lower coal seams.

## 2 Geological Background and Project Profile

The HanJiaWan Coal Mine is situated in the northern part of the ShenFu mining area. It has a production capacity of 4.0 Mt/a and extracts coal from three seams: the 2$^{-2}$ seam, 3$^{-1}$ seam, and 4$^{-2}$ seam. Currently, the mining of the 3$^{-1}$ seam is nearing completion, while the 4$^{-2}$ seam is in the primary stage of mining. The seam have a gentle production slope and are nearly horizontal, with an inclination of approximately 1°. The mining operation follows a downward direction.

The 2$^{-2}$ coal seam is situated in the upper part of the fourth section of the Yan'an Group. The thickness of the coal seam varies from 0.5 to 5.5 m, with an average thickness of 4.06 m. The average depth of the coal seam is 80 m, and it covers a recoverable area of 11 km$^2$. The thickness of the coal seam gradually decreases from west to east. The eastern boundary of the well field is the not mining area, extending along the coal seam strike for 418 m. The room-and-pillar mining area is located between the long-wall mining area and the not mined area, within a width ranging from 135 to 550 m. The long-wall mining area is positioned to the west of the room-and-pillar mining area. The working face has a length of 268 m, a mining height of 4 m, and a strike length of 1820 m. Fully mechanized coal mining with a long wall is employed in the working face, where the entire height is mined at once, and the roof of the mining area is managed using the collapse method.

The thickness of 3$^{-1}$ coal seam ranges from 2.1 to 3.4 m, with an average thickness of 2.9 m. The recoverable thickness is between 1.5 and 3.4 m, with an average of 2.95 m. The burial depth of the coal seam ranges from 101.50 to 157.07 m, and the recoverable area is 12.77 km$^2$. The geological structure of the coal seam is relatively simple, with a local layer of approximately 0.3 m thickness consisting mainly of sandstone. The relationship between the upper and lower coal seams is illustrated in Fig. 1, and the physical and mechanical parameters of the coal seams are presented in Table 1.

## 3 Analysis of Fracture Evolution and Distribution Characteristics of Inter-Layer Rock

Based on the engineering and geological background of HanJiaWan coal mine, this study focus on the distribution characteristics of inter-layer rock fractures during the mining process of the lower coal seam 3302 working face. The study examines the 2$^{-2}$ fully mechanized mining area, room-and-pillar mining area, and not mining area of the upper coal seam separately. Laboratory similar simulation and numerical software calculations are used to analyse and determine the evolution pattern of inter-layer rock fracture when mining the lower coal seam 3302 working face through different mining areas. The objective is to understand the evolution pattern and distribution characteristics of inter-layered fractures in the lower coal seam 3302 workings across different mining areas. Both the laboratory similar simulations and numerical simulation are conducted based on the actual geological conditions in the field. The similar simulation tests platform and numerical model are constructed using the parameters provided in Table 1. The physical similarity simulation test system is illustrated in Fig. 2.

This experiment utilizes a two-dimensional planar physical similarity simulation platform with dimensions of $2000 \times 200 \times 1000$ mm (length, width, and height). The auxiliary monitoring equipment includes a handheld fracture monitor, a digital total station, a stress monitoring acquisition system, and an acoustic emission monitoring system. The handheld fracture monitor is primarily responsible for monitoring and collecting data on microscopic and macroscopic fractures. The digital total station monitors macroscopic fractures and displacements in the inter-layer rock. The acoustic emission monitor is used to monitor all types of fractures (macroscopic, microscopic, and microscopic) within the inter-layer rock. Its working principle involves making the object audible through external conditions and deducing the object's state and changes in internal structure based on its sound. The stress monitoring system

**Table 1** Physical and mechanical parameters of ground

| Stata | Lithology | Thickness /m | Depth /m | Density (kg/m³) | Compressive strength/MPa | Strength of extension/MPa | Elasticity modulus/MPa | Cohesion /GPa | Poisson ratio |
|---|---|---|---|---|---|---|---|---|---|
| Silver sand | | 4.55 | 4.55 | 1850 | 0.9 | 0.05 | 145 | 0.25 | 0.05 |
| Clay | | 18.13 | 22.68 | 1800 | 2.8 | 0.1 | 548 | 0.98 | 0.08 |
| Siltstone | | 1.05 | 23.73 | 2680 | 28.36 | 3.95 | 1420 | 5.1 | 0.25 |
| Post stone | | 1.47 | 25.20 | 2650 | 23.3 | 4.25 | 3765 | 4.3 | 0.23 |
| Mudstone | | 1.42 | 26.62 | 2461 | 21.12 | 1.77 | 1115 | 3.6 | 0.29 |
| Post stone | | 5.99 | 32.61 | 2650 | 23.3 | 4.25 | 3765 | 4.3 | 0.23 |
| Medium sandstone | | 2.15 | 34.76 | 2700 | 32.4 | 2.5 | 6214 | 4.8 | 0.19 |
| Post stone | | 4.64 | 39.40 | 2650 | 23.3 | 4.25 | 3765 | 4.3 | 0.23 |
| Mudstone | | 2.80 | 42.20 | 2461 | 21.12 | 1.77 | 1115 | 3.6 | 0.29 |
| Post stone | | 0.80 | 43.0 | 2650 | 23.3 | 4.25 | 3765 | 4.3 | 0.23 |
| Sandy mudstone | | 1.69 | 44.69 | 2487 | 20.63 | 1.85 | 2875 | 4.7 | 0.24 |
| Post stone | | 4.80 | 49.49 | 2650 | 23.3 | 4.25 | 3765 | 4.3 | 0.23 |
| Sandy mudstone | | 2.60 | 52.09 | 2487 | 20.63 | 1.85 | 2875 | 4.7 | 0.24 |
| Mudstone | | 2.80 | 54.89 | 2461 | 21.12 | 1.77 | 1115 | 3.6 | 0.29 |
| Medium sandstone | | 16.04 | 70.93 | 2700 | 32.4 | 2.5 | 6214 | 4.8 | 0.19 |
| Post stone | | 2.80 | 73.73 | 2650 | 23.3 | 4.25 | 3765 | 4.3 | 0.23 |
| Sandy mudstone | | 0.97 | 74.70 | 2487 | 20.63 | 1.85 | 2875 | 4.7 | 0.24 |
| $2^{-2}$coal | | 4.30 | 79.0 | 1423 | 15.65 | 0.85 | 1376 | 2.2 | 0.28 |
| Siltstone | | 2.78 | 81.78 | 2680 | 28.36 | 3.95 | 1420 | 5.1 | 0.25 |
| Sandy mudstone | | 2.42 | 84.20 | 2487 | 20.63 | 1.85 | 2875 | 4.7 | 0.24 |
| Siltstone | | 3.88 | 88.08 | 2680 | 28.36 | 3.95 | 1420 | 5.1 | 0.25 |
| Mudstone | | 4.35 | 92.43 | 2461 | 21.12 | 1.77 | 1115 | 3.6 | 0.29 |
| Post stone | | 12.0 | 104.43 | 2650 | 23.3 | 4.25 | 3765 | 4.3 | 0.23 |
| Medium sandstone | | 4.30 | 108.73 | 2700 | 32.4 | 2.5 | 6214 | 4.8 | 0.19 |
| $3^{-1}$coal | | 2.90 | 112.93 | 1428 | 16.45 | 1.05 | 1385 | 2.2 | 0.28 |
| Siltstone | | 2.83 | 115.76 | 2680 | 28.36 | 3.95 | 1420 | 5.1 | 0.25 |
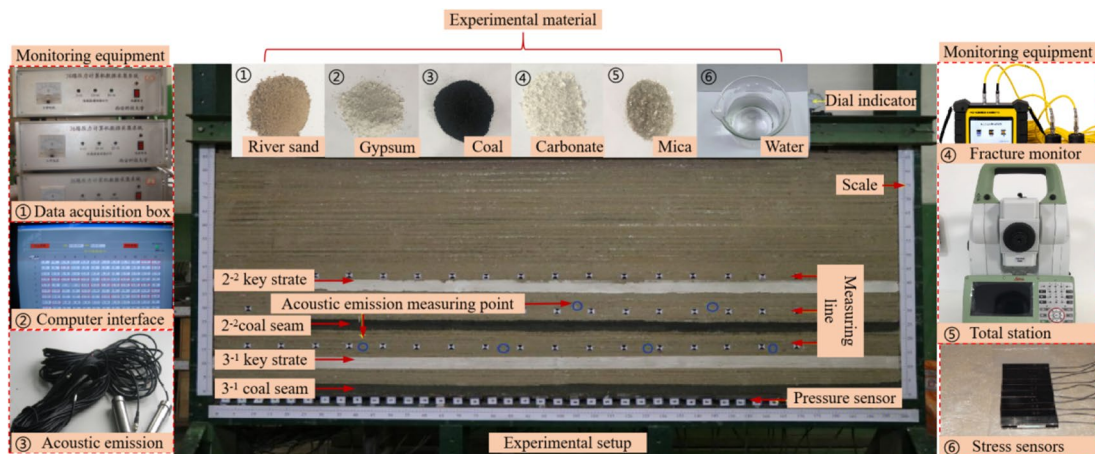


**Fig. 2** Physical similarity simulation experiment system

focuses on monitoring the distribution characteristics and evolution of stress during the mining process of the $2^{-2}$ coal seam and the $3^{-1}$ coal seam. It is primarily distributed in the bottom plate of the $3^{-1}$ coal seam.

The physical similarity simulation test material for the coal rock seam in Hanjiawan coal mine consists primarily of river sand as the main material. Auxiliary materials include gypsum, carbonate, coal, water, and mica flakes. Based on the physical and mechanical parameters provided in Table 1 and the similarity conditions of the coal rock seam (geometric similarity ratio $a_l$: 1:100, time similarity ratio $a_t$: 1:10, and speed similarity ratio $a_v$: 1:10), the ratio of physical similarity simulation test materials for coal rock seam with different rock characteristics is determined. The similarity simulation test platform is constructed using the layer-by-layer compaction method. River sand is used as the aggregate, gypsum, and white powder serve as the cementing

material, coal is used as the main simulation material for the coal seam, and mica flakes are used as the separating material between the interfaces of the coal and rock seams.

The experimental process and main monitoring procedures for coal seam mining are as follows: $2^{-2}$ coal seam comprehensive mining area—$2^{-2}$ coal seam room-and-pillar mining area—$2^{-2}$ coal unmined area—$3^{-1}$ coal comprehensive mining section (comprehensive mining airspace) —$3^{-1}$ coal comprehensive mining section (room-and-pillar mining airspace) —$3^{-1}$ coal comprehensive mining section ($2^{-2}$ coal unmined area). The laboratory conducts similar simulations of the mining process based on the field 3302. The excavation sequence of the working face is determined, with a mining step of 2 m each time, and the room-type mining coal pillar measures $10 \times 10$ m. During the mining process of the working face, the acoustic emission monitor, fracture monitor, and total station are used to primarily monitor and
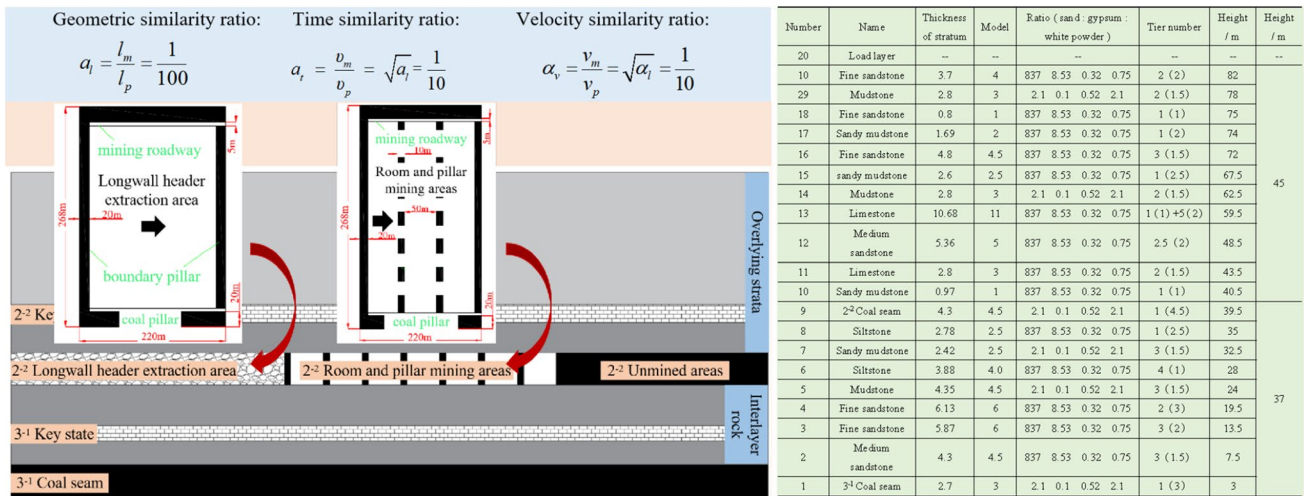
| Number | Name | Thickness of stratum | Model | Ratio (sand : gypsum : white powder) | Tier number | Height / m | Height / m |
|---|---|---|---|---|---|---|---|
| 20 | Load layer | -- | -- | | -- | -- | -- |
| 10 | Fine sandstone | 3.7 | 4 | 837 8.53 0.32 0.75 | 2 (2) | 82 | |
| 29 | Mudstone | 2.8 | 3 | 2.1 0.1 0.52 2.1 | 2 (1.5) | 78 | |
| 18 | Fine sandstone | 0.8 | 1 | 837 8.53 0.32 0.75 | 1 (1) | 75 | |
| 17 | Sandy mudstone | 1.69 | 2 | 837 8.53 0.32 0.75 | 1 (2) | 74 | |
| 16 | Fine sandstone | 4.8 | 4.5 | 837 8.53 0.32 0.75 | 3 (1.5) | 72 | |
| 15 | sandy mudstone | 2.6 | 2.5 | 837 8.53 0.32 0.75 | 1 (2.5) | 67.5 | 45 |
| 14 | Mudstone | 2.8 | 3 | 2.1 0.1 0.52 2.1 | 2 (1.5) | 62.5 | |
| 13 | Limestone | 10.68 | 11 | 837 8.53 0.32 0.75 | 1 (1) +5 (2) | 59.5 | |
| 12 | Medium sandstone | 5.36 | 5 | 837 8.53 0.32 0.75 | 2.5 (2) | 48.5 | |
| 11 | Limestone | 2.8 | 3 | 837 8.53 0.32 0.75 | 2 (1.5) | 43.5 | |
| 10 | Sandy mudstone | 0.97 | 1 | 837 8.53 0.32 0.75 | 1 (1) | 40.5 | |
| 9 | 2-2 Coal seam | 4.3 | 4.5 | 2.1 0.1 0.52 2.1 | 1 (4.5) | 39.5 | |
| 8 | Siltstone | 2.78 | 2.5 | 837 8.53 0.32 0.75 | 1 (2.5) | 35 | |
| 7 | Sandy mudstone | 2.42 | 2.5 | 2.1 0.1 0.52 2.1 | 3 (1.5) | 32.5 | |
| 6 | Siltstone | 3.88 | 4.0 | 837 8.53 0.32 0.75 | 4 (1) | 28 | |
| 5 | Mudstone | 4.35 | 4.5 | 2.1 0.1 0.52 2.1 | 3 (1.5) | 24 | 37 |
| 4 | Fine sandstone | 6.13 | 6 | 837 8.53 0.32 0.75 | 2 (3) | 19.5 | |
| 3 | Fine sandstone | 5.87 | 6 | 837 8.53 0.32 0.75 | 3 (2) | 13.5 | |
| 2 | Medium sandstone | 4.3 | 4.5 | 837 8.53 0.32 0.75 | 3 (1.5) | 7.5 | |
| 1 | 3-1 Coal seam | 2.7 | 3 | 2.1 0.1 0.52 2.1 | 1 (3) | 3 | |

**Fig. 3** Physical similarity simulation experiment material properties and test process

analyze the fracture distribution characteristics and evolution law of the inter-layers. The stress monitoring system continuously monitors the experimental process to capture the stress distribution characteristics. The physical similarity simulation experiment material properties and test process are illustrated in Fig. 3.

The numerical simulation was performed using the UDEC discrete element numerical calculation software. The model was established based on the characteristics of the rock stratum, as indicated by the column diagram of No.8 borehole of Hanjiawan Mine, and the parameters of each coal rock in Table 1. The size of the model was designed to be 150 m × 134 m (length × width). Since the $2^{-2}$ seam and $3^{-1}$ seam are shallow buried coal seams, the horizontal stress was set to be 1.25 times the vertical stress. The overlying rock layer was simplified in the modeling process, and the unit size of the model was divided based on the physical and mechanical properties and thickness of each rock layer. To analyze the deformation, yielding, and damage state of different rock seams in detail, the unit size varies and is determined according to the strength of the rock seam. The specific coal rock parameters and coal seam arrangement are determined based on Table 1. The numerical calculation is constructed using a Moore Cullen model in the YZ direction. In the distance of the $2^{-2}$ coal seam from the upper surface is set to 80 m, the inter-layer distance between the $2^{-2}$ coal seam and the $3^{-1}$ coal seam is set to 35 m. These values are determined based on the actual geologic conditions of the Hanjiawan Coal Mine and the characteristics of coal seam distribution. The UDEC discrete element numerical modeling is illustrated in Fig. 4. The rock mechanical parameters used in the numerical simulation are provided in Table 2.

Since the rock layer at the coal mine site contains a significant number of joints and natural fissures, contact surfaces are introduced between the layers of rock to realistically simulate the development of fissures and the movement of the rock layer. The boundary condition of the numerical model is set to leave a 15 m boundary coal pillar on each side of the model. The mining process begins by sequentially mining 3 m to complete the $2^{-2}$ coal seam, followed by mining the $3^{-1}$ coal seam. The main focus of this numerical simulation is to study the development of inter-layer rock fractures in the upper and lower coal seams. By monitoring the number of contacts between the inter-layer rock seams damaged under the three types of mining airspace formed during the mining of the lower group $3^{-1}$ coal seam by the upper group coal mining, the mechanism of inter-layer rock fracture development is explored. This analysis involves comparing the patterns of inter-layer rock fracture development and distribution characteristics.
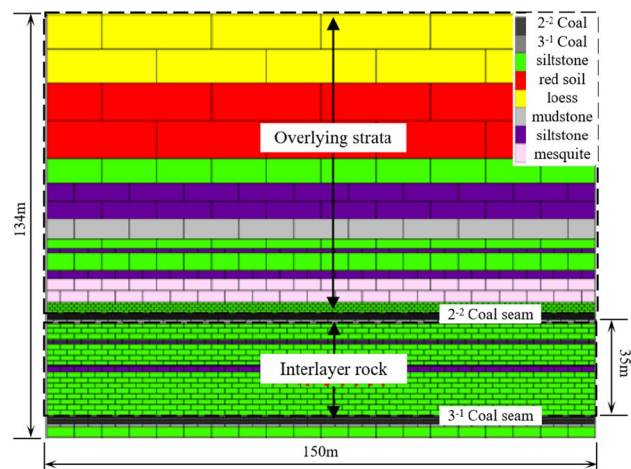


**Fig. 4** UDEC discrete element numerical modeling

**Table 2** Numerical simulation of mechanical parameters

| Rock name | Volumetric weight (kg/m³) | Volume modulus (MPa) | Shera modulus (MPa) | Poisson ratio | Tensile strength (MPa) | Cohesion (MPa) | Fraction angle (deg) |
|---|---|---|---|---|---|---|---|
| Coal seam | 1350 | 2381 | 1163 | 0.29 | 0.8 | 1.3 | 33 |
| Silt stone | 2500 | 3372 | 3816 | 0.14 | 1.2 | 4.5 | 21 |
| Medium sandstone | 2350 | 2204 | 1723 | 0.19 | 0.9 | 1.8 | 32 |
| Fine-grained sandstone | 2600 | 9302 | 9137 | 0.13 | 2.1 | 4.2 | 28 |
| Mesquite | 2600 | 2135 | 1668 | 0.19 | 0.6 | 1.0 | 34 |
| Mud-stone | 2300 | 2895 | 2930 | 0.2 | 1.5 | 2 | 30 |

## 3.1 Evolution and Distribution Characteristics of Fractures in Inter-Layer Rock of Fully Mechanized Mining Area

When the lower group 3302 working face is mined under the upper coal $2^{-2}$ coal fully mechanized mining area, the development and distribution characteristics of the fractures in the inter-layer rock are shown in Fig. 5.

The characteristics of fracture development at the early stage of mining are shown in Fig. 5a. At the early stage of mining in the lower coal seam, the inter-layer rock has tiny transverse separation fractures. When the breaking strength



(a) In the early stage



(b) In the middle stage



(c) In the late stage
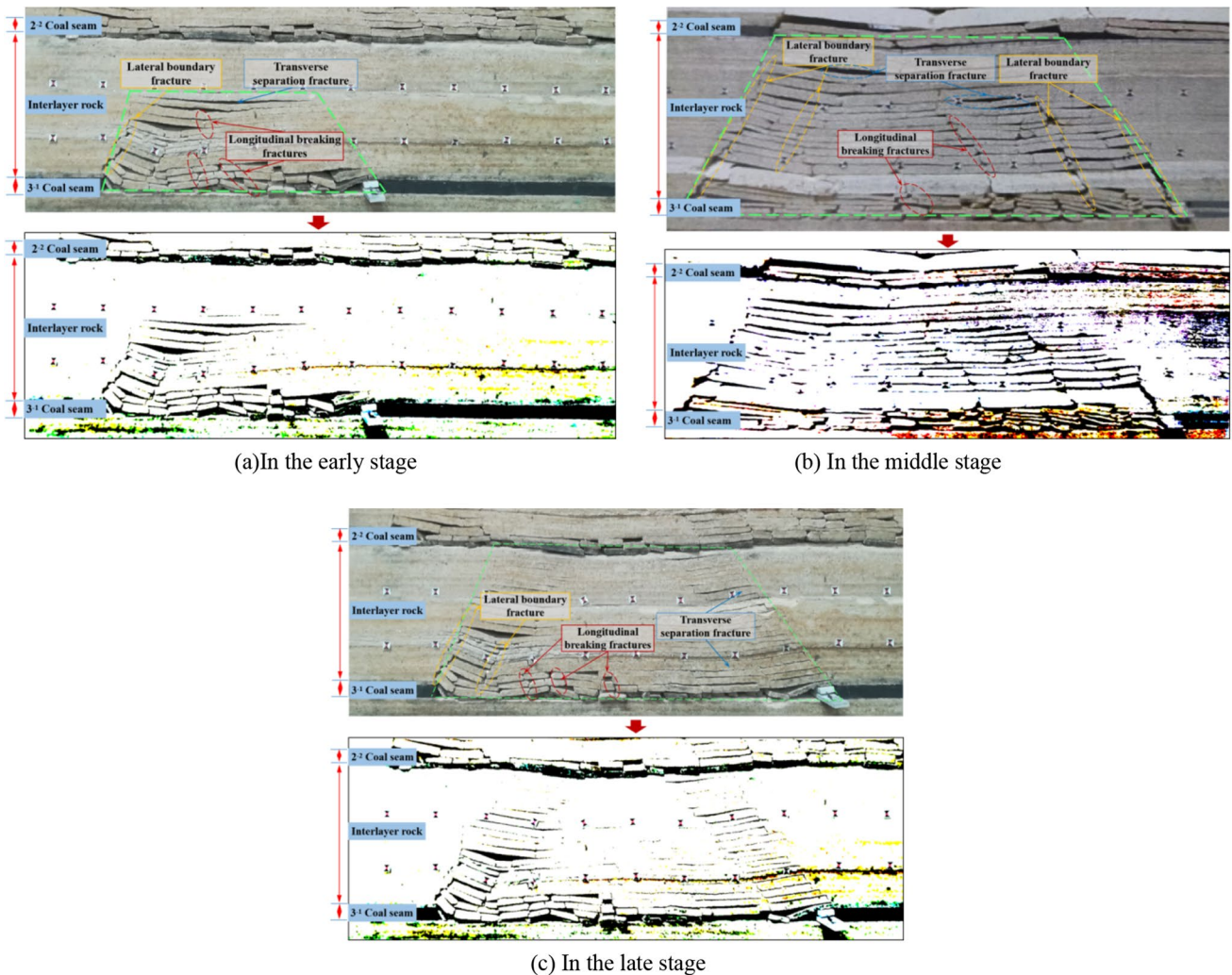
**Fig. 5** Similar simulation of inter-layer rock fracture development and distribution characteristics

(a) Upper seam mining



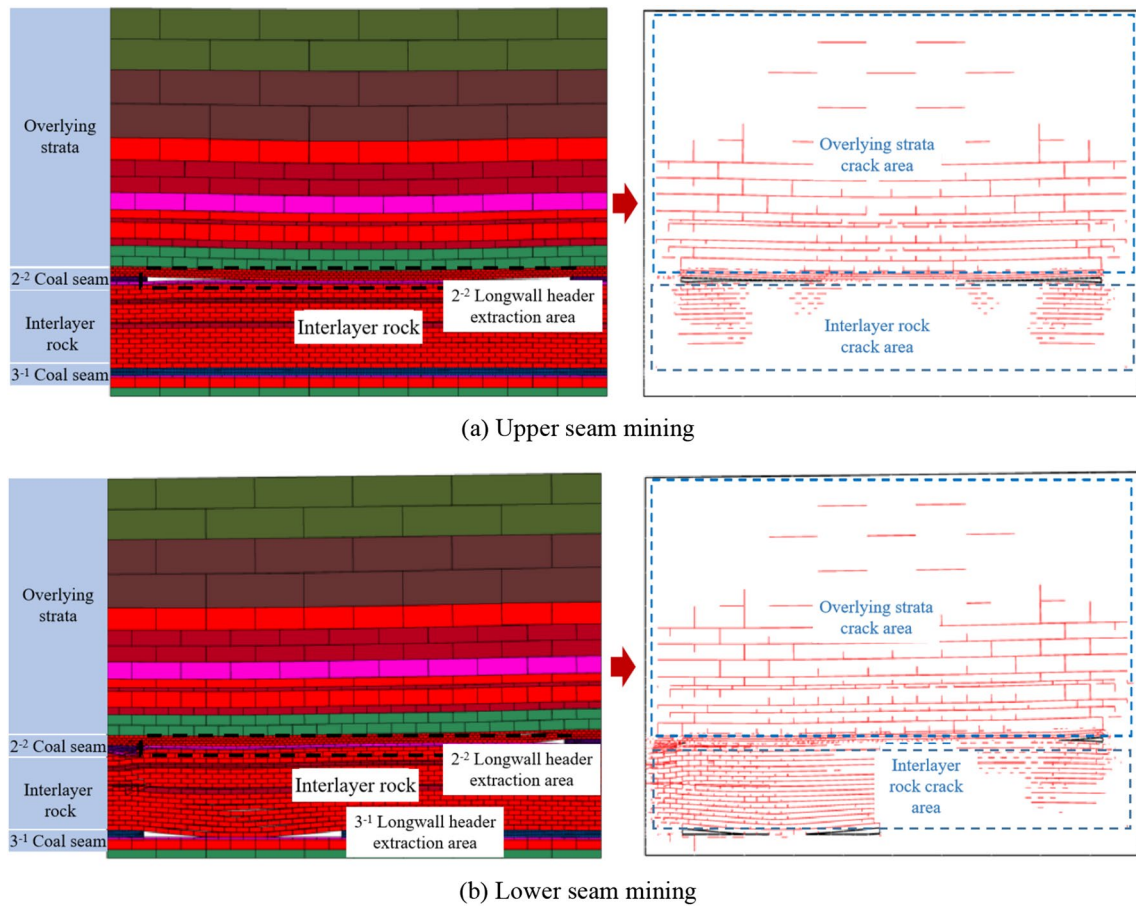(b) Lower seam mining

**Fig. 6** Numerical simulation of inter-layer rock fracture development and distribution characteristics



(a) Inter-layer rock fractures do not penetrate the mining area



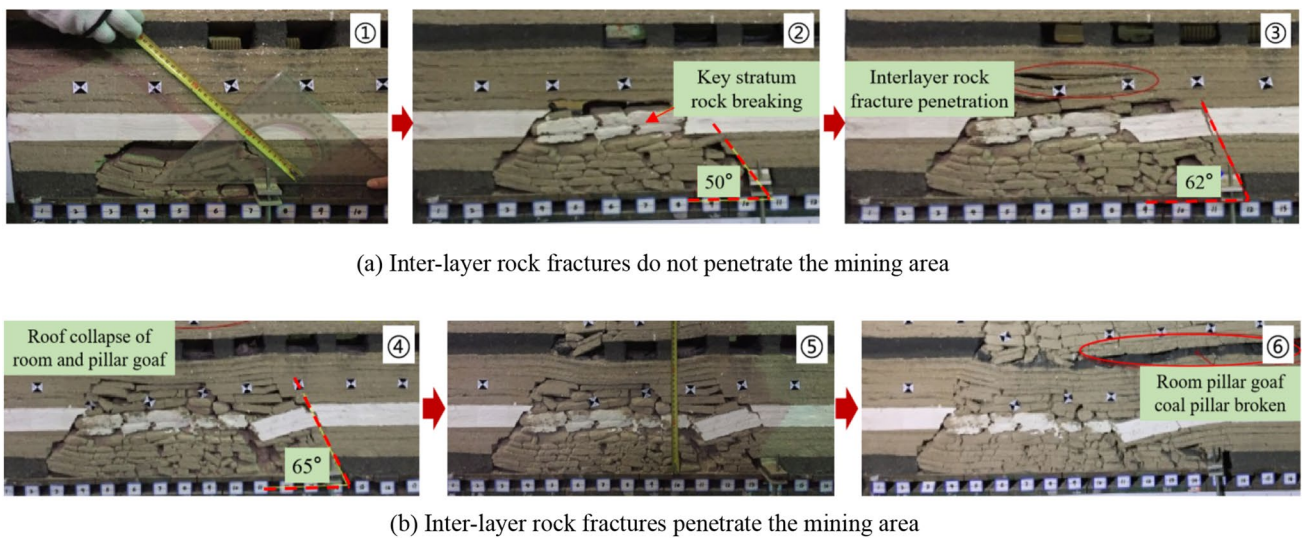(b) Inter-layer rock fractures penetrate the mining area

**Fig. 7** Similar simulation of fracture development and distribution characteristics of inter-layer rock under room-and-pillar area

of the inter-layer rock layer exceeds the ultimate shear strength, longitudinal breaking fractures appear, and the inter-layer rock gradually forms longitudinal and transverse through fractures. When the rock stratum breaks periodically, the width of transverse breakage fractures increases, the development height increases, the longitudinal breakage fractures pass through, and the breakage spacing is similar to the step distance of the periodic pressure. The width and number of fractures on the open-off cut side of the lower seam at the early stage of mining are larger than those on the face side. The maximum development height of the fractures is about 22 m, and the distribution of fractures in the inter-layers is approximately in the shape of a positive trapezoid.

The development and distribution characteristics of inter-layer rock fractures during the middle stage of mining are shown in Fig. 5b. The longitudinal breakage fractures show an obvious periodic distribution, and the width and number of these fractures are larger than those of the central breakage fractures at the side of the open-off cut and working face. The width of transverse separation fractures is greater in the upper part than in the lower part, and the maximum height of fracture development is 35 m, extending up to the upper coal seam mining area. The number and density of inter-layer fractures are significantly greater than those at the beginning of mining, and the overall pattern of fracture development is positively trapezoidal.

The development and distribution characteristics of inter-layered rock fractures in the late stage of mining are shown in Fig. 5c. As the working face of the lower coal seam is mined, the overlying rock layer significantly influences the development of the inter-layer rock fractures, as these fractures are connected with the upper mining area. The transverse separation fractures in the middle of the inter-layered rock have closed, and both the fracture density and fracture width have decreased. The longitudinal breaking fractures have partially closed due to the turning back of the breaking inter-layered rock and the loading of the overlying rock mass. The degree of development of inter-layer fractures on the side of the open-off cut and the side of the working face is significantly larger than that in the middle part. The middle part of the inter-layer fractures is gradually closing, and the development pattern shows a positive trapezoidal shape. The degree of fracture development is smaller than that in the middle stage.

To accurately depict the evolution of the fracture development and distribution characteristics of the inter-layered rock, numerical simulation was used for analysis. The specific evolution process and distribution characteristics are shown in Fig. 6.

Figure 6a displays the fracture development process and distribution characteristics of the inter-layered rock and overlying rock layer during the mining of the $2^{-2}$ coal seam of the upper group. The fracture development characteristics are essentially similar to the results of similar simulation tests. Through the numerical simulation cloud diagram, it can be clearly observed that the mining of the upper group of coal seams significantly influences the development of fractures in the inter-layered rock. The development of fractures in the inter-layered rock is particularly noticeable in the lower part of the side of the open-off cut and the side of the working face mining, with a development depth of about 15 m. The depth of the central part of the development is about 9 m, and the density and width of the fractures are greater than those in the central part of the location.

Figure 6b displays the numerical simulation cloud map of the development and distribution characteristics of the inter-layered rock cracks during the mining process of the lower coal seam. When the lower seam is mined to the middle position, the overall development and distribution characteristics of the inter-layered rock fractures are highly similar to the results of similar simulation tests. The transverse separation fractures and longitudinal breakage fractures penetrate through the inter-layered rock. The longitudinal breakage fractures are periodically distributed, and the inter-layered rock fractures are larger at the upper position than at the lower position. This accurately reflects the development and distribution of fractures in the inter-layer rock, and verifies the consistency with the development of cracks in the inter-layer rock during the field mining process.

## 3.2 Evolution and Distribution Characteristics of Fractures in Inter-Layer Rock of the Room and Pillar Mining Area

When the lower group 3302 working face is mined under the upper group $2^{-2}$ coal room-and-pillar mining area, the development and distribution characteristics of inter-layer rock fractures are shown in Fig. 7.

Figure 7a illustrates the development process and distribution characteristics of the inter-layer rock fractures before they penetrate the upper mining area. At the early stage of mining, the fracture development is similar to the fully mechanized mining area, with transverse separation fractures. Longitudinal breaking fractures are formed when the ultimate strength of the inter-layer rock layer is less than

the breaking strength. In the middle stage of mining, the key layer between the layers breaks to form transverse separation fractures and longitudinal fractures. The width and density of the fractures increase significantly, and huge separation fractures are formed under the key rock layers. In the late stage of mining, the transverse cracks of the inter-layer rock rapidly expand upward, connecting with the upper group of room-and-pillar mining area. The density and width of the fractures in the lower part of the inter-layer rock are larger than those in the upper part of the rock layer.

Compared with the evolution characteristics of the inter-layer fractures under the fully mechanized mining area, the periodicity of the development of longitudinal breakage fractures and lateral boundary breakage fractures is not obvious. However, the fracture width and density are significantly larger than those of the cracks in the rock under the fully mechanized mining area. The morphology of the fracture development in the inter-layer rock is similar to the fully mechanized mining area, which are all in positive trapezoidal shape.

Figure 7b illustrates the development process and distribution characteristics of the fractures in the inter-layer rock after penetration with the upper mine area. As the working face of the lower coal seam is mined, the upper transverse separation fractures and longitudinal breakage fractures of the inter-layer appear to close. Under the influence of the load of the overlying rock layer, the stress is gradually transferred to the coal pillar of the mining area and fractures appear. At this time, the density and width of the fractures in the lower rock layer of the inter-layer rock are larger than those in the upper rock layer.

When the continuity of the coal pillar in the room-and-pillar mining area is damaged, the development of longitudinal fractures in the inter-layer rock shows periodic evolution. The location of longitudinal fractures is situated in the middle of the room-and-pillar mining area. The width and density of the cracks in the inter-layer rock are larger than those in the fully mechanized mining area, and the development pattern of the fractures is not obvious.

To realistically depict the fracture development and distribution characteristics of the inter-layered rock under the room-and-pillar mining area, we refer to Fig. 8a. This figure shows the fracture development and distribution characteristics of the inter-layer rock and overlying rock layer after room-and-pillar mining of the upper coal seam. It can be observed that the overlying rock layer has slight transverse separation fractures. The fractures in the lower inter-layered rock of the room-and-pillar mining area are primarily transverse separation fractures, supplemented by longitudinal

breakage fractures. The depth of fracture development is about 3 m, and the width and density of the transverse separation fractures are larger than those of the longitudinal breakage fractures.

Figure 8b illustrates the development and distribution characteristics of the inter-layer rock fractures after mining the $2^{-2}$ coal seam of the upper group to form a room and pillar mining area. During the mining of the lower coal seam, the degree of development of inter-layer rock fractures is significantly greater than that of inter-layer rock cracks under the fully mechanized mining area. Its distribution characteristics are basically consistent with the results of similar simulation experiments, featuring irregular distribution of transverse separation fractures and longitudinal breakage fractures. Generally, the width and density of transverse separation fractures are greater than those of longitudinal breakage fractures.

### 3.3 Comparative Analysis of Fracture Evolution and Distribution Characteristics of Inter-Layer Rock

Through quantitative comparative analysis of the evolution pattern and distribution characteristics of fractures in the aforementioned inter-layered rock under different mining areas, this paper introduces the concept of rock damages degree (Bai et al. 2016; Bai and Tu 2020). The rock damage degree is used as a quantitative criterion to characterize the degree of fracture development in the inter-layered rock. The rock damage degree is defined as the ratio of the sum of the contact lengths of tensile damage and shear damage occurring in the rock in the monitoring area during coal seam mining to the total contact length of the rock in the monitoring area. The calculation formula is shown in Eq. (1). The tensile damage degree is calculated as the ratio of the contact length of tensile damage to the total contact length of the monitored area, as shown in Eq. (2). Similarly, the degree of shear damage is calculated as the ratio of the contact length of shear damage to the total contact length of the monitored area, as shown in Eq. (3).

$$K_d = \frac{c_t + c_s}{c_0} \times 100\% \tag{1}$$

$$K_t = \frac{c_t}{c_0} \times 100\% \tag{2}$$

$$K_s = \frac{c_s}{c_0} \times 100\% \tag{3}$$

(a) Upper seam mining



(b) Lower seam mining
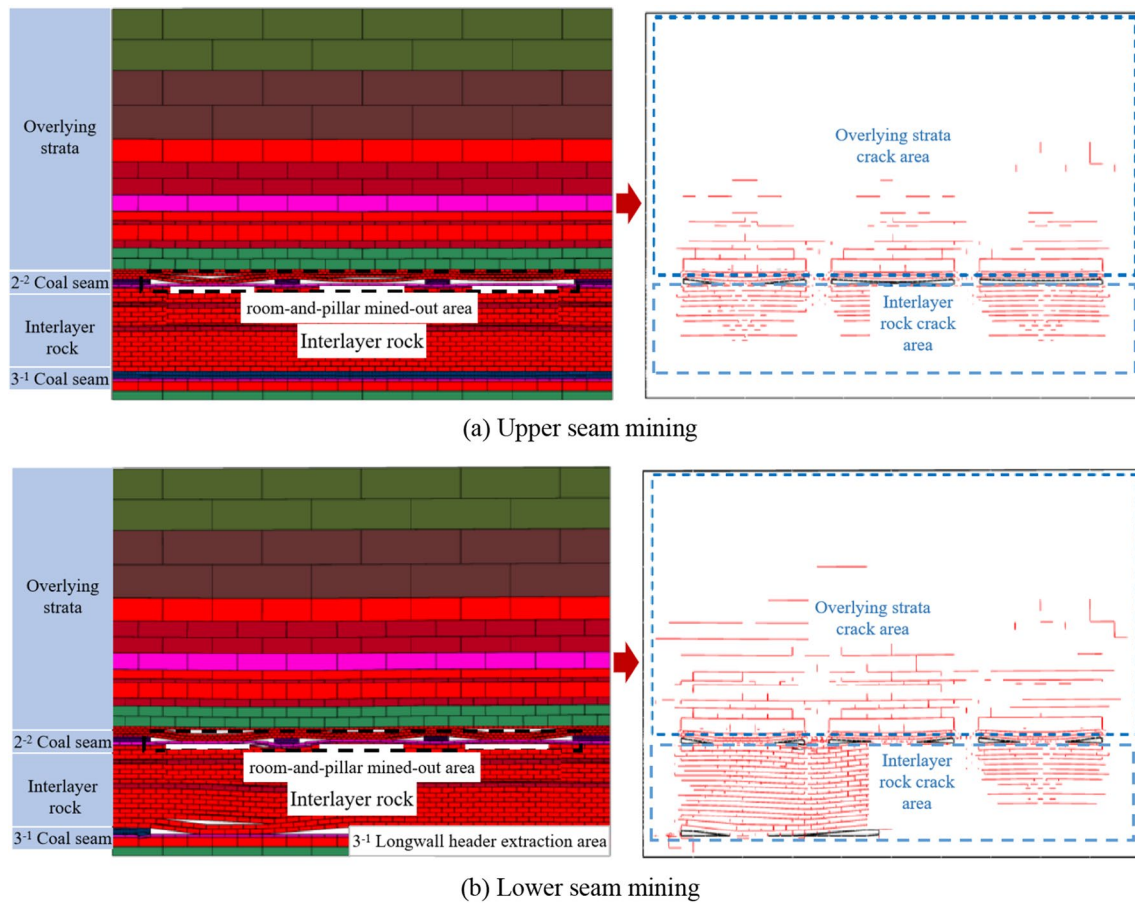
**Fig. 8** Numerical simulation of fracture development and distribution characteristics of inter-layer rock under room-and-pillar mining area

where $K_d$ is the degree of rock damage; $K_t$ is the degree of rock tensile damage; $K_s$ is the degree of rock shear damage; $c_0$ is the length of total contact in the rock, m; $c_t$ is the length of contact where tensile damage occurs in the rock, m; $c_s$ is the length of contact where shear damage occurs, m.

Through continuous monitoring of the damage contact length of the inter-layer rock fractures under the longwall fully mechanized mining area and room and pillar mining area, the variation in rock damage of the inter-layered rocks under these mining methods was obtained, as shown in Fig. 9. The scatter plot in Fig. 9 illustrates that the overall damage to the inter-layered rock under the fully mechanized mining area is less than that under the room-and-pillar mining area. In addition, after the formation of different mining areas in the upper group of coal seams, the damage to the inter-layered rock gradually increase towards the fully mechanized mining workings of the lower group of coal seams. The degree of damage to the inter-layered rock below the room-and-pillar

mining area is greater in shear than in tension, indicating that the development of fractures in the inter-layered rock is primarily influenced by shear damage. In contrast, the degree of shear damages is greater than tensile damage to the inter-layered rock below the fully mechanized mining area. This suggests that the fracture development in the inter-layered rock is mainly driven by shear damage, although it is less pronounced compared to the shear damage observed in the inter-layered rock in the room-and-pillar mining area. Inter-layer rock crack damage length monitoring is mainly determined using various methods such as acoustic emission in similar simulation experiments and plastic zone and displacement cloud mapping in numerical simulations.

To accurately and quantitatively characterize the variation of damage in inter-layered rocks during the mining of the upper group of coal seams and the lower group of coal seams, as well as the proportion of shear damage and tensile damage in each mining process. The proportion of
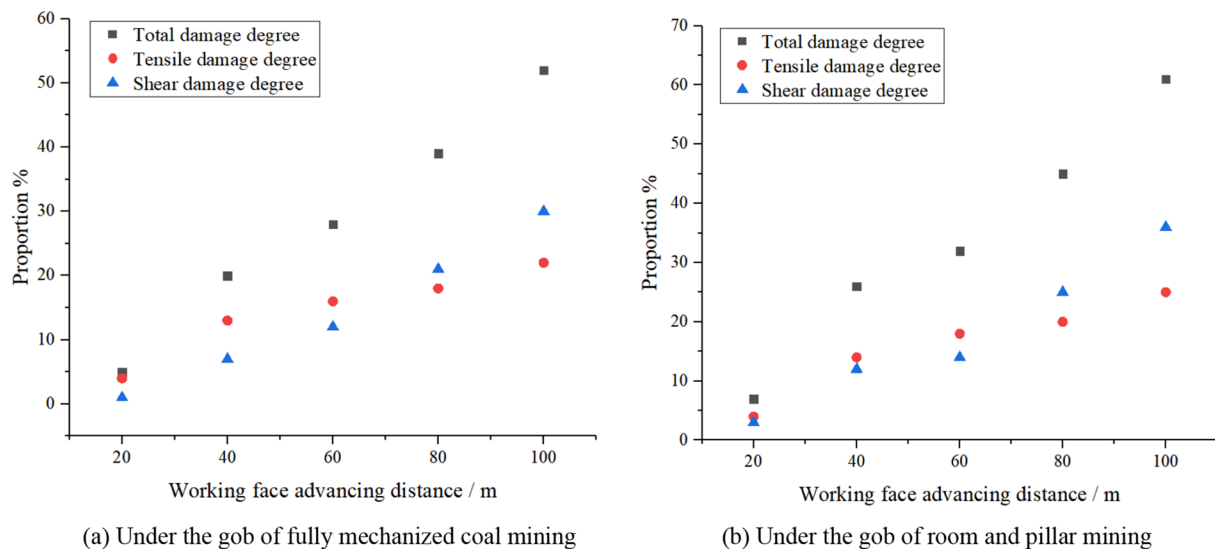
(a) Under the gob of fully mechanized coal mining

(b) Under the gob of room and pillar mining

**Fig. 9** Scatter plot of damage degree change of inter-layer rock mass in different area

the monitoring results is shown in Fig. 10. From Fig. 10a, it can be observed that the degree of fracture damage in inter-layered rock varies significantly before and after repeated mining under the long wall fully mechanized mining area. After mining the upper group of coal seams, the degree of damage to the inter-layered rock is approximately 14%, while after mining the lower group of coal seams, it increases to approximately 52%. Shear damage degree dominates in both cases, accounting for approximately 22% and 30% respectively. As depicted in Fig. 10b, the variation in the degree of fracture damage to the inter-layered rock before and after repeated mining under the room-and-pillar mining area is more compared to the long wall fully mechanized mining area. After mining the upper group of coal seams, the degree of damage to the inter-layered rock is approximately 18%, while after mining the lower group of coal seams, it increases to approximately 61%. Shear damage dominates in both cases, accounting for approximately 25% and 36% respectively. It is evident that when the upper group coal is mined by room-and-pillar mining and long-wall fully mechanized mining, the former experiences more damaged than the latter during the mining process of the lower group coal seam. The room-and-pillar mining area has a significant influence on the development of inter-seam rock fractures, resulting in more developed. Therefore, when mining the coal seam under the room-and-pillar mining area in the lower group working face, it is crucial to pay attention to the development of fractures the inter-layer rock.

## 4 Analysis of the Mechanism of Fracture Formation in Inter-Layered Rock

### 4.1 Analysis of the Mechanism of Rock Fractures Development Between Seams Mined in the Upper Group of Coal Seams

#### 4.1.1 Analysis of Inter-Layered Rocks Stress and Depth of Damage Under Different Mining Methods

When the upper group coal seam is mined using long-wall fully mechanized coal mining and room-and-pillar coal mining methods, they produce different disturbance effects on the inter-layered rock. As a result, the fracture evolution pattern and distribution characteristics of the inter-layered rock exhibit distinct expansion phenomena. These phenomena can be clearly observed through similar simulation test and numerical calculation. In the case of mining, the upper group coal seam using the long wall fully mechanized coal mining method, the stress state and fracture development form of the bottom plate of the upper group coal seam and the upper position of the inter-layered rock differ due to being in different mining stages. With long-wall fully mechanized coal mining, the stress in the upper part of the inter-layered rock undergoes a sequence of increasing compression, expansion, and recovery. The transverse separation fractures experience a cycle of closing, opening, and closing, while the longitudinal breaking fractures go through opening, closing, and opening. This results in the formation of compression region, expansion region, transition region, and re-compacted region within the inter-layered rock. On the other hand, when the upper group of coal seam are mined using room-and-pillar mining, only the compression region and expansion region are formed in

(a) Under fully mechanized mining area

(b) Under the room and pillar area
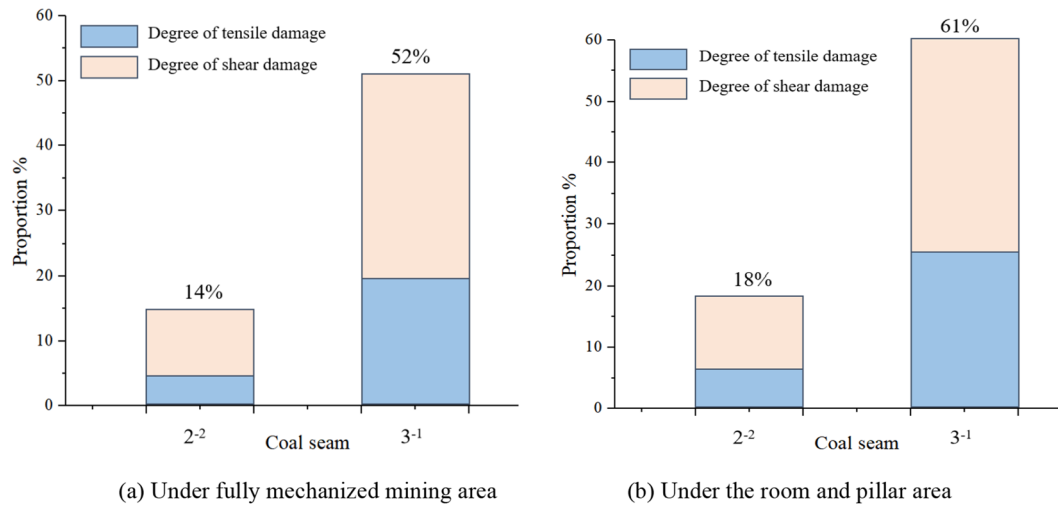
**Fig. 10** The damage histogram of different positions of inter-layer rock mass during the mining of upper and lower coal seams

the upper position of the inter-layered rock. The inter-layered rock below the coal pillar forms the compression region, while the inter-layered rock below the room-and-pillar mining area becomes the expansion region.

(1) Analysis of inter-layer rock stress and damage depth in long-wall fully mechanized mining. Based on the elasticity theory and the Mohr–Coulomb strength criterion, the damage depth of the inter-layered rock caused by mining the upper group of coal seams during long-wall fully mechanized coal mining is calculated and analyzed using the slip line calculation theory. The process of inter-layered rock damages is illustrated in Fig. 11.

The logarithmic double helix equation for $r$, $r_0$, can be expressed as:

$$r = r_0 e^{\theta \tan \phi_d} \tag{4}$$

Approximating the curve in portion of the region shown in Fig. 11 as a straight line of solution, the geometric relationship in the figure can be expressed as follows:

$$r_0 = x_a / 2 \cos \left( \frac{\pi}{4} + \frac{\phi_d}{2} \right) \tag{5}$$

$$\alpha = \frac{\pi}{2} - \left( \frac{\pi}{4} - \frac{\phi_d}{2} - \theta \right) \tag{6}$$

$$\sin \alpha = \cos \left( \alpha - \frac{\pi}{2} \right) \tag{7}$$

$$h_m = r \sin \alpha \tag{8}$$

The equation based on the cohesion of the coal seam $C$ as parameter $x_a$ is:

$$x_a = \frac{M}{2\eta \tan \phi} \ln \frac{k\gamma H + C \tan \phi}{\eta C \tan \phi} \tag{9}$$

By substituting Eqs. (4) to (7) and (9) into Eq. (8) based on the basic parameters of coal rock mechanics, we can obtain the maximum depth of damage $h_m$ to the bottom slab as follows:

$$h_m = \frac{M \cdot \cos \phi_d}{4\eta \cdot \tan \phi \cdot \cos \left( \frac{\pi}{4} + \frac{\phi_d}{2} \right)} e^{\left( \frac{\pi}{4} + \frac{\phi_d}{2} \right) \tan \phi_d} \cdot \ln \frac{k\gamma H + C \cdot \cot \phi}{\eta \cdot C \cdot \cot \phi} \tag{10}$$

where: $M$ is the mining height of the coal seam, m; $k$ is the stress concentration factor; $\phi$ is the internal friction angle of the coal seam, °; $H$ is the mining depth, m; $\eta = \frac{1+\sin\phi}{1-\sin\phi}$ is the triaxial stress factor; $\gamma$ is the average capacity weight of the overlying rock seam, $kN/m^3$; $\phi_d$ is the internal friction angle of the inter-layered rock, °; $C$ is the cohesion of the coal seam, $MPa$; $x_a$ is the length of the yield region of the coal seam, m.

According to the mechanical parameters of the upper group $2^{-2}$ coal in Table 1 and the geological conditions of the mine, we can analyze and calculate the depth of damage to the inter-layered rock seam during long-wall fully mechanized coal mining of the upper group coal, the mining height of the $2^{-2}$ coal $M = 4.3$ m, the internal friction angle of the rock layer $\phi_d = 30°$, the triaxial stress coefficient $\eta = \frac{1+\sin 36°}{1-\sin 36°} = 3.88$ of the overlying rock layer, the internal friction angle $\phi = 36°$ of the coal seam, the stress concentration coefficient $k = 2.4$ of the upper group coal, the average capacity weight $\gamma = 25\,kN/m^3$ of the overlying rock layer, the burial depth of the upper group coal $H = 80$ m, the cohesive force of the coal seam $C = 2.2$. Substituting each parameter into Eq. (10):
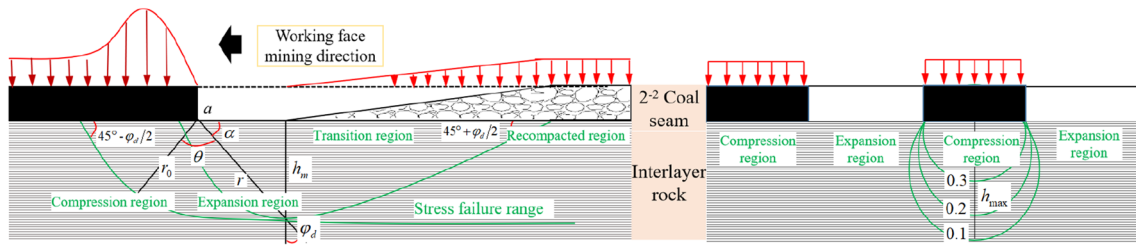
**Fig. 11** Upper group coal seam mining inter-layer rock mass should stand and partition diagram

$$h_m = \frac{4.3 \times \cos 30°}{4 \times 3.88 \times \tan 36° \times \cos\left(\frac{\pi}{4} + \frac{\pi}{6}{2}\right)} e^{\left(\frac{\pi}{4} + \frac{\pi}{6}{2}\right)\tan 30°}$$

$$\times \ln \frac{2.4 \times 25 \times 80 + 2.2 \times \cot 36°}{3.88 \times 2.2 \times \cot 36°}$$

$$= 22.7 \text{ m.}$$

(2) Room and pillar mining inter-layer rock stress analysis. When mining the upper group of coal seams using room-and-pillar mining, the stress distribution law below the upper position of the inter-layered rock, specifically in the room-and-pillar mining area, is analyzed. The stress distribution of the coal pillar at the upper position of the inter-layered rock is considered a plane strain problem. The research focuses on the coal pillar and the inter-layered rock, and the inter-layer rock force model and damage depth are shown in Fig. 12.

According to the constructed mechanical model, the stress at any point $M(x, z)$ within the inter-layer rock is solved by considering the micro-length $d\xi$ at a distance $\xi$ from the origin $O$. Based on the half-plane theory, the stress at the point $M$ can be obtained as follows:

$$\begin{cases} \sigma_x = -\frac{2}{\pi} \int_{-a/2}^{a/2} \frac{qz(x-\xi)^2}{[z^2+(x-\xi)^2]^2} d\xi \\ \sigma_z = -\frac{2}{\pi} \int_{-a/2}^{a/2} \frac{qz^3}{[z^2+(x-\xi)^2]^2} d\xi \\ \tau_{xz} = -\frac{2}{\pi} \int_{-a/2}^{a/2} \frac{qz^2(x-\xi)}{[z^2+(x-\xi)^2]^2} d\xi \end{cases} \quad (11)$$

For the solution of Eq. (11), the permutation method is used with permutation parameters $\frac{z-x}{t} = \xi$ and $t$. The negative sign in the above equation indicates that the direction of the load is opposite to the direction of the coordinate axis, the solution yields:

$$\begin{cases} \sigma_x = \left\{ -\frac{q}{\pi} \left[ \frac{z(x-\xi)}{z^2+(x-\xi)^2} - \arctan\frac{x-\xi}{z} \right] \right\} \Big|_{-a/2}^{a/2} \\ \sigma_z = \left\{ -\frac{q}{\pi} \left[ \frac{z(x-\xi)}{z^2+(x-\xi)^2} + \arctan\frac{x-\xi}{z} \right] \right\} \Big|_{-a/2}^{a/2} \\ \tau_{xz} = \left\{ \frac{q}{\pi} \left[ \frac{z(x-\xi)}{z^2+(x-\xi)^2} \right] \right\} \Big|_{-a/2}^{a/2} \end{cases} \quad (12)$$

For the determination of $q$ in the above equation, room and pillar mining will transfer the overlying rock seam load

to the coal pillar, so it can be seen as the overlying load acting equivalently and equally on its coal pillar, then the load acting on the coal pillar is:

$$q = p - p_0 = \gamma H \left( \frac{b}{a} + \frac{a}{L} + \frac{b^2}{La} \right) \quad (13)$$

where $\gamma$ is the capacity of the overlying rock seam, $kN/m^3$; $H$ is the average depth of burial of the room mining workings, $m$; $a$ the width of the coal pillars in the room and pillar mining area, $m$; $b$ is the distance between the coal pillars, $m$; $L$ is the length of the coal pillars, $m$.

$$\begin{cases} \sigma_x = -\frac{(Lb+a^2+b^2)\gamma H}{\pi La} \left[ \arctan\frac{x+a/2}{z} - \arctan\frac{x-a/2}{z} - \frac{z(x+a/2)}{z^2+(x+a/2)^2} + \frac{z(x-a/2)}{z^2+(x-a/2)^2} \right] \\ \sigma_z = -\frac{(Lb+a^2+b^2)\gamma H}{\pi La} \left[ \arctan\frac{x+a/2}{z} - \arctan\frac{x-a/2}{z} + \frac{z(x+a/2)}{z^2+(x+a/2)^2} - \frac{z(x-a/2)}{z^2+(x-a/2)^2} \right] \\ \tau_{xz} = \frac{(Lb+a^2+b^2)\gamma H}{\pi La} \left[ \frac{z^2}{z^2+(x+a/2)^2} - \frac{z^2}{z^2+(x-a/2)^2} \right] \end{cases} \quad (14)$$

From Eq. (14), a stress contour plot of the room-and-pillar mining coal pillar against the inter-layered rock is obtained, as shown in Fig. 12b. The green curve indicates the horizontal stress contour, and the black curve indicate the vertical stress contour. The stress in the inter-layered rock is primarily in the horizontal direction when its distance from the central pillar is greater than the width of the pillar. In this case, the stress in the inter-layered rock is less than $0.2q$. On the other hand, the stress in the inter-layered rock is primarily in the vertical direction when its distance from the vertical direction is greater than twice the width of the pillar. In this case, the stress in the inter-layered rock is less than $0.3q$. The vertical stress is the greatest at any depth directly below the centre of the pillar. The stress in the inter-layered rock is mainly influenced by the vertical stress, the horizontal stress have less influence.

According to the production situation of the HanJiaWan coal mine room and pillar mining site, using Mathematic software, the stress cloud diagram of the coal pillar transferring load onto the inter-layers rock can be obtained, as shown in Fig. 13.

As can be seen from the stress contour of inter-layer rock in Hanjiawan Coal Mine, the stress contour diagram of the coal pillar of the inter-layered rock in the upper group of coal

**Fig. 12** Mechanical model and stress transfer isobar of inter-layer rock mass in room-pillar gob

( a ) Mechanical model

( b ) Stress transfer isobar

(a) Horizontal stress contour cloud diagram

(b) Vertical stress contour cloud diagram

(c) Shear stress contour cloud diagram
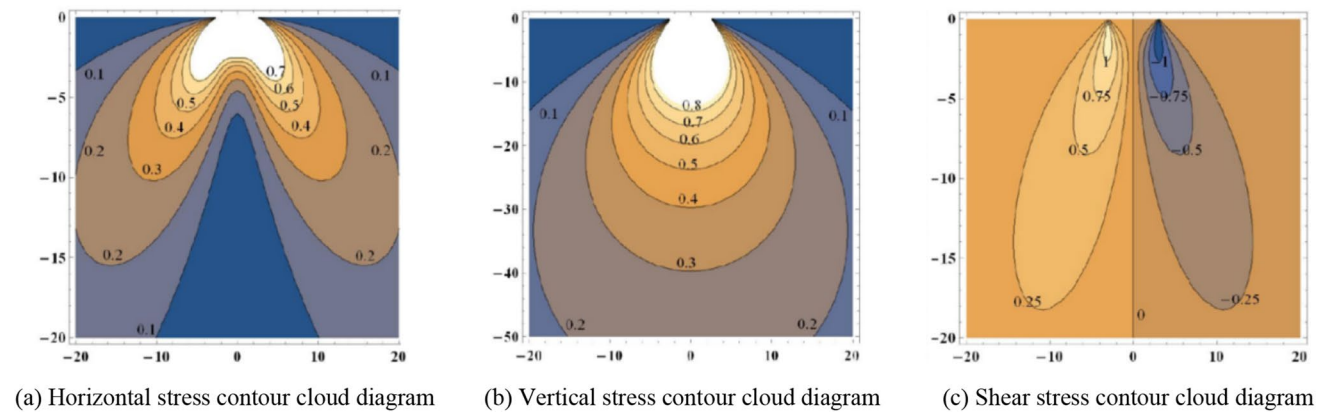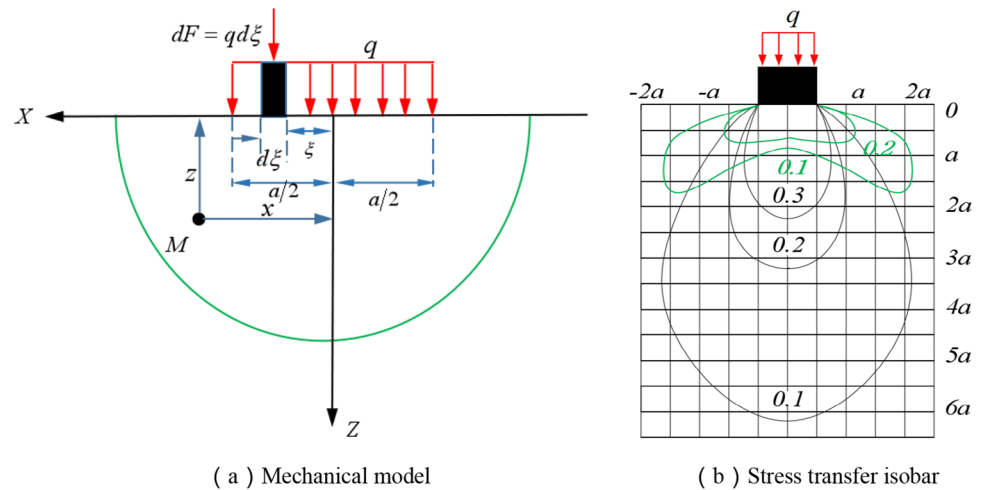
**Fig. 13** Stress contour of inter-layer rock in Hanjiawan Coal Mine

seams shows a 'alveolar' shape in the horizontal direction, and a 'light bulb' shapes in the vertical direction. The shear stresses contours in the inter-layered rock exhibit a 'biplane' shape. As the depth increases, the horizontal stresses in the inter-layered rock become less influential in the horizontal direction. The attenuation of horizontal stresses is more pronounced in the center of the coal pillar compared to the sides. The vertical stress in the inter-layered rock gradually decrease with increasing depth. However, the decrease in the vertical direction is much less than in the horizontal direction. The shear stresses in the inter-layered rock are symmetrically distributed over the centre of coal pillar. This indicates that the shear stresses have equal magnitude and opposite direction on each side of the symmetry about the column, decreasing towards the lower left and right corners.

(3) Room and pillar mining inter-layer rock damage depth analysis. After the room and pillar mining the upper group of coal seam, the load of the coal pillar is transferred downwards, causing damage to the inter-layered rock and compromising

its integrity. Under the concentrated load of the upper group of room-and-pillar coal pillars, the maximum shear stress in the inter-layered rock is located at a depth of half the width of the coal pillars. Based on the above calculation results and considering the self-weight stress $\gamma z$ in the inter-layered rock itself, the principal stress at any point in the inter-layered rock in the plane strain state is:

$$\begin{cases} \sigma_1 = \frac{p}{\pi}(\alpha + \sin \alpha) + \gamma z \\ \sigma_3 = \frac{p}{\pi}(\alpha - \sin \alpha) + \gamma z \end{cases} \tag{15}$$

Damage to inter-layered rock under multi-directional stress obeys the Mohr–Coulomb damage criterion:

$$\sigma_1 - \xi \sigma_3 = R_c \tag{16}$$

Substituting Eq. (15) into Eq. (16) to collate gives:

$$z = \frac{p}{\pi \gamma}\left(\frac{\xi + 1}{\xi - 1}\sin \alpha - \alpha\right) - \frac{R_c}{\gamma(\xi - 1)} \tag{17}$$

Through $\frac{dz}{d\alpha} = 0$, the maximum depth of damage $h_{\max}$ of the inter-layer rock is obtained as:

$$\frac{dz}{d\alpha} = \frac{p}{\pi\gamma}\left(\frac{\xi+1}{\xi-1}\cos\alpha - 1\right) = 0 \tag{18}$$

It is possible to obtain:

$$\cos\alpha = \frac{\xi-1}{\xi+1} \tag{19}$$

The calculation gives:

$$\alpha = \cos^{-1}\frac{\xi-1}{\xi+1} \tag{20}$$

Substituting Eq. (20) into Eq. (17) gives the maximum depth of damage to the inter-layer rock beneath the coal pillar as:

$$h_{\max} = \frac{p}{\pi\gamma}\left(\frac{2\sqrt{\xi}}{\xi-1} - \cos^{-1}\frac{\xi-1}{\xi+1}\right) - \frac{R_c}{\gamma(\xi-1)} \tag{21}$$

Substituting $p = \gamma H\left(1 + \frac{b}{a} + \frac{a}{L} + \frac{b^2}{La}\right)$, Eq. (21) can be expressed as:

$$h_{\max} = \frac{(La + Lb + a^2 + b^2)H}{\pi La}\left(\frac{2\sqrt{\xi}}{\xi-1} - \cos^{-1}\frac{\xi-1}{\xi+1}\right) - \frac{R_c}{\gamma(\xi-1)} \tag{22}$$

where: $a$ is the width of the coal pillar, m; $b$ is the width of the coal room, m; $L$ is the length of the coal pillar, m; $R_c$ is the uniaxial compressive strength of the upper position of the inter-layered rock, $MPa$; $H$ is the burial depth of the overlying coal seam, m; $\gamma$ is the average allowable weight of the overlying rock, $kN/m^3$; $\xi = \frac{1+\sin\phi_d}{1-\sin\phi_d}$; $\phi_d$ is the angle of internal friction of the inter-layered rock.

According to the mechanical parameters of the upper group $2^{-2}$ coal rock seam in Table 1 and the geological conditions of the mine, the analysis and calculation of the damage depth of the inter-layered rock during coal mining in the upper group room-and-pillar coal mining type is performed. The width of the coal pillar $a = 6$ m, the width of the coal house $b = 6$ m, the length of the coal pillar $L = 6$ m, the average uniaxial compressive strength $R_c = 25.6MPa$ of the inter-layered rock layer, the burial depth $H = 80$ m of the upper group coal seam, the average rock mass capacity $\gamma = 25kN/m^3$, $\xi = \frac{1+\sin 30°}{1-\sin 30°} = 3$ of the overlying rock layer, the angle of internal friction $\phi_d = 30°$ of the inter-layered rock.

$$h_{\max} = \frac{(6\times6 + 6\times6 + 6^2 + 6^2)\times80}{3.14\times6\times6}\left(\frac{2\sqrt{3}}{3-1} - \cos^{-1}\frac{3-1}{3+1}\right) - \frac{25.6}{25(3-1)}$$

$$= 28.7 \text{ m.}$$

### 4.1.2 Mechanics of Fracture Evolution of Inter-Layered Rocks Under Different Mining Methods

By analyzing the stress and damage depth of the inter-layer rock during the mining of the upper group coal seam, it is observed that different stress partitions are formed in the inter-layered rock during room-and-pillar mining and longwall fully mechanized mining of the upper group coal seam. This variation in stress partitions leads to different mechanical mechanisms in the evolution of fractures in the inter-layered rock. Specifically, when the inter-layered rock is in the compression region, the fractures bend and expand on higher stress states (Zhang et al. 2015). No fractures closure, when $\sigma_1 \leq \frac{4G_0}{k+1}$ and $\sigma_{3m} \leq \frac{4G_0}{k+1}\alpha$. $k$ is $3 - 4v$ in the plane strain state and $k$ is $\frac{3-v}{1+v}$ in the plane stress state. $v$ is the Poisson's ratio, $G_0$ is the shear modulus of the rock between the layers, $\sigma_{3m}$ is the lateral stress at the unloading point, $\sigma_1$ is the maximum principal stress, and $\alpha = b/c$, $c$ and $b$ are the half-length axis and half-openness of the elliptical fracture, respectively. Schematic modeling of inter-layer rock fracture evolution, as shown in Fig. 14.

When the inter-layer rock is in the compression region, as shown in Fig. 14a. The conditions under which bending and extension of fractures occur in the compression region of inter-layered rock are:

$$\sigma_1 = \frac{\sqrt{3}K_{ICC}}{2F(\theta)\sqrt{\pi c}} + \sigma_3 \tag{23}$$

The mean open displacement of primary fractures (Basista and Gross 1998; Zhou et al. 2005) is:

$$b = \frac{\pi c(1 - v_0^2)}{E_0}\left(\tau_{eff} - \sigma_3 l_1 \cos\theta\right) \tag{24}$$

where $F(\theta) = \sin\theta\cos\theta$; $K_{ICC}$ is the fracture toughness of the formation, $K_{ICC} = K_I$; $F = 2c\tau_{eff}$; $l_1$ is the length of the secondary fracture; $E_0$ is the modulus of elasticity of the rock mass; $\theta$ is the angle between the fracture and the direction of the principal stress; $\sigma_3$ is the minimum principal stress; $\tau_{eff}$ is the effective shear stress of the rock mass between the layers that actually produces frictional sliding, $\tau_c$ is the cohesion; $\mu$ is the coefficient of friction, $\tau_{eff} = (\sigma_1 - \sigma_3)\cos\theta\sin\theta - \tau_c - \mu(\sigma_3\sin^2\theta + \sigma_1 + \cos^2\theta)$.

When the inter-layered rock is in the transition region, as shown in Fig. 14b. The lateral stress within the transition region of the inter-layered rock remains relatively stable, while the vertical stress decreases significantly. This stage can be considered as the process of unloading the perimeter pressure and vertical stress of the inter-layered rock. The expansion of fractures in the inter-layered rock primarily occurs in the form of reverse slip (Zhou and Zhang 2007).
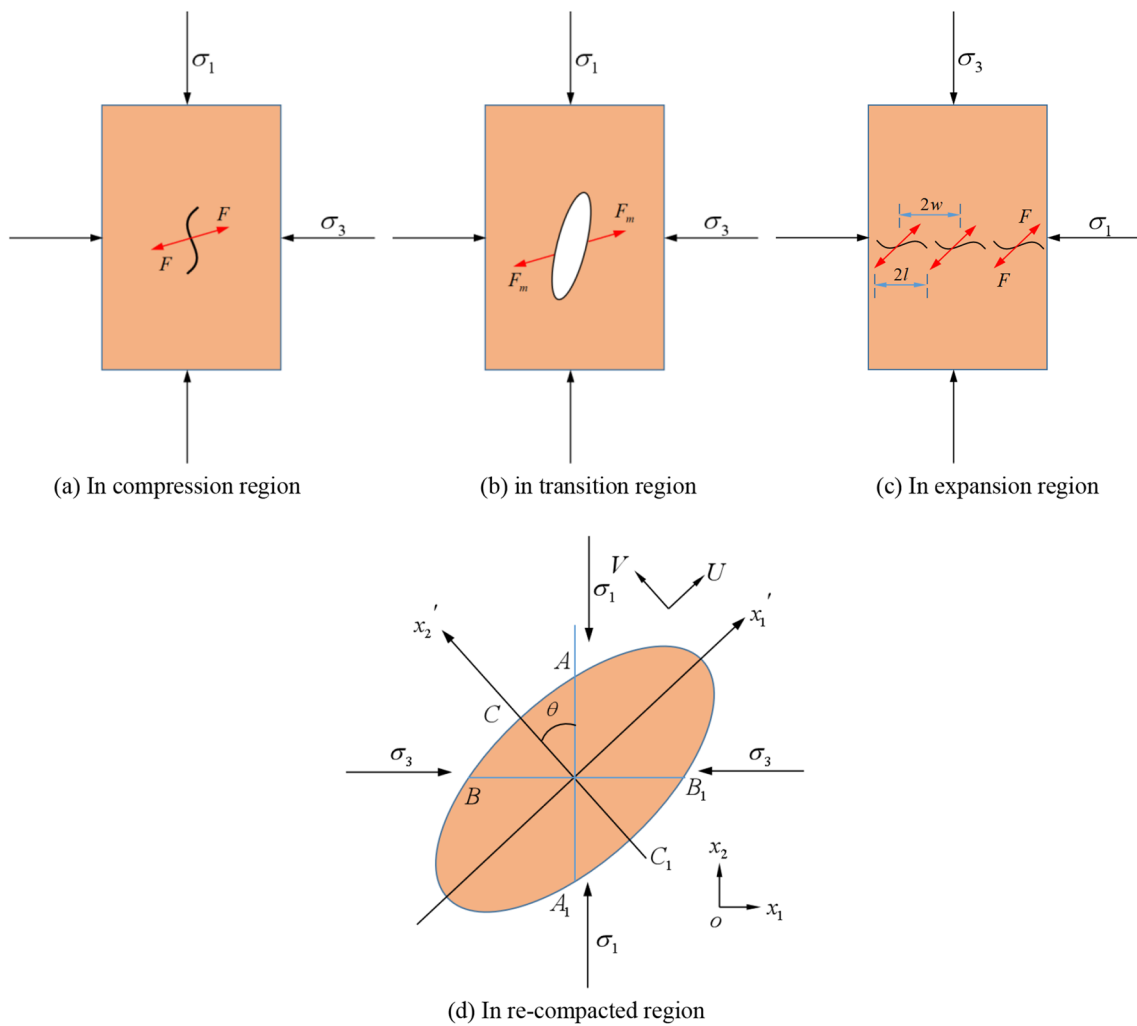
(a) In compression region     (b) in transition region     (c) In expansion region



(d) In re-compacted region

**Fig. 14** Schematic diagram of fracture stress evolution in different regions

When $\sigma_1 < \frac{4G_0}{k+1}\alpha$, the wedge force $F_m$ on the fractures at the start of the unloading is:

$$F_m = 2\cos\theta\left\{-\mu\left[\left(\sigma_{3m} - \frac{4G_0\alpha}{k+1}\right)\cos^2\theta + \sigma_{1m}\sin^2\theta\right] - \tau_c\right\}$$
$$+ 2\cos\theta\left[\frac{1}{2}(\sigma_{1m} - \sigma_{1c} - \sigma_{3m})\sin 2\theta\right] \tag{25}$$

The wedge force $F_u$ at any point during the unloading of the inter-layer rock is:

$$F_u = \left\{2\mu\cos\theta\left[\left(\sigma_3 - \frac{4G_0\alpha}{K+1}\right)\cos^2\theta + \sigma_{1m}\sin^2\theta\right] + \tau_c\right\}$$
$$+ 2\cos\theta\left[\frac{1}{2}(\sigma_1 - \sigma_{1c} - \sigma_{3m})\sin 2\theta\right] \tag{26}$$

When reverse slip $F_m = F_u$ occurs in the inter-layer rock, then the critical stress for reverse slip is obtained as:

$$\sigma_1 = \left[\frac{\sigma_2\sin 2\theta}{2} - \mu\left(\sigma_3 - \frac{8G_0\alpha}{k+1}\right)\cos^2\theta - 2\left(\tau_c + \mu\sigma_{1m}\sin^2\theta\right)\right] \Big/ \left(\cos\theta\sin\theta + \mu\cos^2\theta\right) \tag{27}$$

where $\sigma_{1m}$ is the axial stress at the starting point of unloading; $\sigma_{1c}$ is the average maximum principal stress in the rock between layers.

When the inter-layer rock is in the expansion region, as shown in Fig. 14c. In this region, the vertical stress in the inter-layered rock decreases to zero or becomes tensile stress, destabilization and expansion of the fracture occurs when the $\sigma_1 > \frac{4G_0}{k+1}\alpha > \sigma_3$ frictional bending fracture occurs.

Type II open displacements of primary fractures in inter-layered rock are:

$$\overline{b_2} = \frac{\pi(1-v^2)}{E_0}\left[\frac{\sqrt{\pi l}}{\sqrt{\omega\sin\frac{\pi l}{\omega}}}\pi_{eff} - \sigma_3\frac{\sqrt{2\omega\tan\frac{\pi l}{\omega}}}{\sqrt{\pi l}}\overline{l}\cos\theta\right] \tag{28}$$

The vertical stress required for the unstable expansion of fractures in the inter-layer rock is:

$$\sigma_3 = \left\{ -k\sqrt{w} + 2c\sin\theta_1 \left[ \tau_c + (\sigma_1 - \sigma_{1c}) \times \sin\theta_1(\mu\sin\theta_1 - \cos\theta_1) \right] \right\} \bigg/ \left[ \sqrt{2}\omega + c\sin 2\theta_1(\mu\cos\theta_1 + \sin\theta_1) \right] \tag{29}$$

where $\bar{l}$ is the average length of the fracture; $\omega$ is the half-length of the fracture spacing between two mutual fractures. When $\sigma_1 < \frac{4G_0}{k+1}\alpha$ the fracture does not bend and expand, but reverse slip and open deformation of the fracture occurs.

When the inter-layer rock is in the re-compaction region, as shown in Fig. 14d. In these regions, the vertical stresses gradually re-compact and close the previously generated open fractures. The fracture in the inter-layer rock is considered completely closed when the relative displacement between points $C$ and $C_1$ is assumed to be equal to the opening of the fracture $2b$. The critical closure condition of the fracture is:

$$\sigma_{1c} + \sigma_{3c} = \frac{8G_0}{k+1}\alpha - (\sigma_{1c} - \sigma_{3c})(1+\alpha)\cos 2\theta \tag{30}$$

where $\sigma_{3c}$ is the average minimum principal stress in the inter-layer rock. The closure displacement of the inter-layer rock fracture in the longitudinal and transverse directions is:

$$\begin{cases} U_2^{x_2} = \frac{k+1}{4G_0}\left[ f_1(\theta)\sigma_1 + g_1(\theta)\sigma_3 \right]c \\ U_2^{x_1} = \frac{k+1}{4G_0}\left[ f_2(\theta)\sigma_1 + g_2(\theta)\sigma_3 \right]c \end{cases} \tag{31}$$

where, $f_1(\theta) = \sin\theta\cos\beta_1 + 2\sin\beta_1\cos\theta$, $g_1(\theta) = -\sin\theta\cos\beta_1$, $f_2(\theta) = -\cos\theta\cos\beta_2$, $g_2(\theta) = \cos\theta\cos\beta_2 - 2\sin\beta_2\sin\theta$. The critical angle of closure of a fracture can be expressed as:

$$\theta_c = 0.5\arccos\frac{\frac{8G_0}{k+1}\alpha - (\sigma_1 + \sigma_2)}{(\sigma_2 - \sigma_1)(1+\alpha)} \tag{32}$$

By studying the expansion of fractures in the compression region, expansion region, transition region, and re-compacted region of the inter-layered rock under different mining methods of the upper group coal seam, we have constructed fracture development models for the inter-layered rock at different stress regions during the mining process. We have determined critical conditions for fracture expansion, fracture opening displacement, and other parameters. In addition, we have analyzed the dynamic evolution process of the fracture development in the inter-layered rock under different mining regions for the upper group coal seam. Through this analysis, we have determined the fracture development mechanism of the inter-layered rock under the influence of mining for the upper group coal seam.

## 4.2 Analysis of the Mechanism Of Rock Fractures Development Between Seams Mined in the Lower Group of Coal Seams

### 4.2.1 Analysis of the Height of Fracture Development in Inter-Layered Rocks Mined in the Lower Group Coal Seam

During the mining process of the lower group coal seam, the inter-layer rock structure undergoes destabilization and collapse due to the overlying load stress and self-weight stress. This leads to further development of fractures in the inter-layered rock due to repeated disturbances. To analyze the height of the inter-layer rock collapse in the lower group coal seam mining, it is necessary to consider the comprehensive mining height $M_Z$ instead of just the height of a single coal seam. The height of the overburden fracture zone and collapse zone in the lower group coal seam can be expressed according to the "three lower" coal mining operation regulations as follows:

$$M_Z = M_2 + \left( M_1 - \frac{L}{y_2} \right) \tag{33}$$

where $M_1$ is the mining height of the upper group of coal seams, m; $M_2$ is the mining height of the lower group of coal seams, m; $L$ is the distance between the rock seams of the seams, m; $y_2$ is the ratio of the mining collapse height to the mining height of the lower group of coal seams.

To analyse the height of fracture development in the inter-layered rock during repeated mining of the lower group coal seam, we can refer to the calculation method for the development height of the "collapse zone" and "hydraulic fracture zone" in the overlying rock under repeated disturbance from the lower group coal seam. By comparing the development height of the "two zones" with the thickness of the inter-layered rock, we can determine the fracture development height in the inter-layered rock under the repeated disturbance of the lower coal seam. This method provides a basis for determining the fracture development mechanism in the inter-layered rock under different mining methods, and helps determine the development mechanism of transverse separation fractures and longitudinal breaking fractures in the inter-layered rock during mining (Table 3).

**Table 3** Fracture development height of inter-layer rock mass under repeated mining

| "Two-band" | Lithology | Suitable for $M \le 3$ m coal seam | "Two-band" | Lithology | Suitable for $M \le 3$ m coal seam | |
| --- | --- | --- | --- | --- | --- | --- |
| | | Formula one | | | Formula one | Formula two |
| Caving zone height | Stiffness | $H_k = \frac{100M}{2.1M+16} \pm 2.5$ | Height of Fractured water-conducting zone | Stiffness | $H_{li} = \frac{100M}{1.2M+2.0} \pm 8.9$ | $H_{li} = 30\sqrt{M} + 10$ |
| | Medium-hard | $H_k = \frac{100M}{4.7M+19} \pm 2.2$ | | Medium-hard | $H_{li} = \frac{100M}{1.6M+3.6} \pm 5.6$ | $H_{li} = 20\sqrt{M} + 10$ |
| | Weakness | $H_k = \frac{100M}{6.2M+32} \pm 1.5$ | | Weakness | $H_{li} = \frac{100M}{3.1M+5.0} \pm 4.0$ | $H_{li} = 10\sqrt{M} + 5$ |
| | Very soft | $H_k = \frac{100M}{7.0M+63} \pm 1.2$ | | Very soft | $H_{li} = \frac{100M}{5.0M+8.0} \pm 3.0$ | – |

$M$ is the effective mining height, the lithology strength is classified according to the uni-axial compressive strength of the rock, with 40–80 MPa for hard, 20–40 MPa for medium-hard, 10–20 MPa for soft and 10 MPa or less for very soft

### 4.2.2 Mechanisms of Inter-Layered Rock Fracture Development in Lower Coal Seam Mining

During the mining of the lower group of coal seams, the inter-layered rock structure undergoes fracturing. This results in the formation of transverse separation fractures and longitudinal breaking fractures. Transverse separation fractures typically occur at the contact surfaces between different rock layers in the inter-layered rock structure, while longitudinal breaking fractures occur within rock layer along its longitudinal section. Since the elastic modulus and thickness of each rock layer composing the inter-layer rock are different, transverse separation fractures and longitudinal breakage fractures are formed in the deformation and destruction process of the inter-layer rock. Transverse separation fractures include tension horizontal off-layer fractures and shear staggered fractures, and longitudinal breakage fractures include longitudinal tension fractures and longitudinal shear fractures.

When there is a significant difference in bending stiffness between the rock layers within the inter-layer, synchronous bending and deformation of these layers becomes challenging. As a result, separation occurs at the contact surface of the adjacent rock layers, leading to the formation of tension horizontal off-layer fractures, as depict in Fig. 15a. Conversely, if each rock layer within the inter-layer undergoes synchronous bending and deformation, horizontal shear stress is generated at the contact surface of each adjacent rock layer. When this horizontal shear stress is exceeds the shear strength of the contact surface, horizontal shear staggered fractures emergence along the contact surface, as illustrated in Fig. 15b. In the longitudinal direction, there are vertical shears stresses and horizontal positive stresses between the layers within the inter-layer rock, formation of longitudinal tension fractures and longitudinal shear fractures along the longitudinal direction, as depicted in Fig. 15c. The vertical shear stress of each rock layer within the inter-layer seam is highest in the middle of the rock layer, while the horizontal positive stress is highest at the surface of the rock layer.

The distribution of positive and shear stresses is illustrated in Fig. 15d. When the horizontal tensile stress exceeds the tensile strength of the rock layer, tension fractures occur within the rock layers within the inter-layer rock. As tension fractures develop, the effective bearing area between the rock layers decreases, leading to an increase in shear stress along the longitudinal section. When the shear strength of the rock layers within the inter-layer is lower than the shear stress, longitudinal penetration fractures occur along the longitudinal section.

1. Tension off-layer fractures

Because of the variability in the modulus of elasticity and thickness of the various rock layers that make up the inter-layer rock, the inter-layer rock is assumed to be a combined rock beam structure. When mining the lower group of coal seam workings, tension fractures between the layers within the inter-layered rock seam. These fractures are formed when the tensile stress within the inter-layered exceeds the bonding force between the layers, under the influence of the overlying rock load and self-weight stress. As the mining space gradually increases, these tension fractures continue to develop.

Conditions for the formation of transverse separation fracture at the contact surface of each rock layer within the inter-layer are as follows:

$$\tau' = c' + \sigma_n \tan \theta' \tag{34}$$

where $\theta'$ is the angle of internal friction at the rock contact surface; $c'$ is the cohesion at the rock contact surface; $\tau'$ is the shear stress at each rock contact surface; $\sigma_n$ is the normal stress at the rock contact surface.

The determination of whether adjacent rock layers form a separated space is based on the examination of the maximum curvature and maximum deflection of each adjacent rock layer within the inter-layer as it undergoes sinking, the criterion for determining this can be expressed as follows:
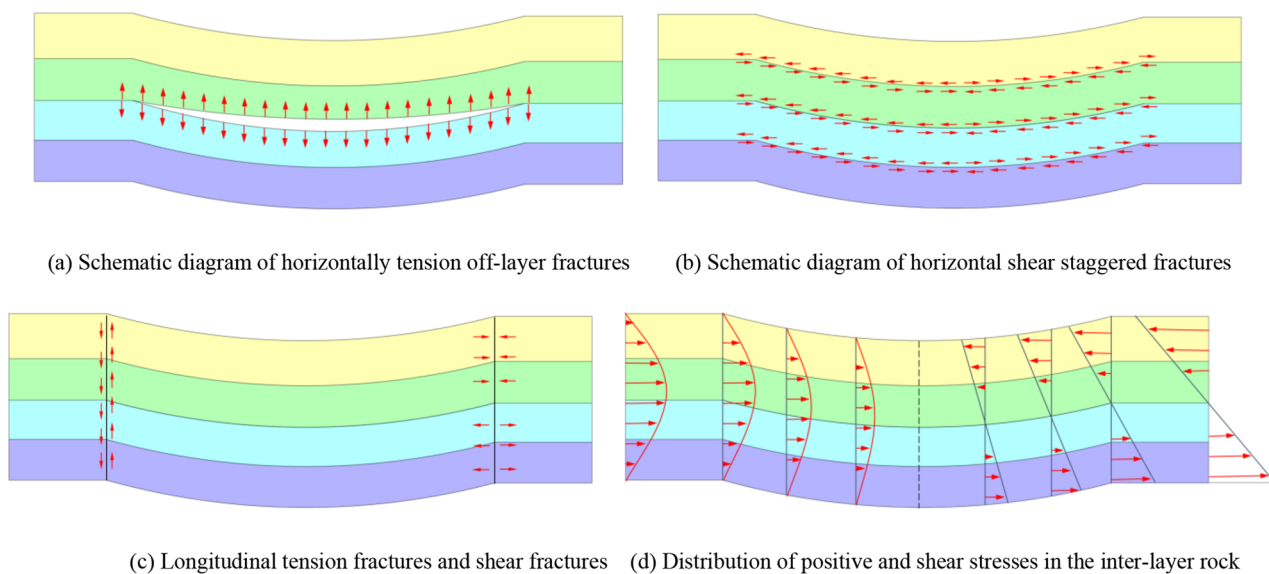
(a) Schematic diagram of horizontally tension off-layer fractures

(b) Schematic diagram of horizontal shear staggered fractures

(c) Longitudinal tension fractures and shear fractures

(d) Distribution of positive and shear stresses in the inter-layer rock

**Fig. 15** Horizontal separation and longitudinal fracture stress distribution of inter-layer rock strata

$$\rho_{max} = \alpha' \frac{\gamma L^2}{Em^2} \tag{35}$$

$$\omega_{max} = \beta' \frac{\gamma L^4}{Em^2} \tag{36}$$

where $\alpha'$, $\beta'$ is the coefficient of determination of the support conditions of the rock beam in the inter-layer; $\gamma$ is the capacity weight of the rock formation, $kN/m^3$; $L$ is the span of the rock beam, m; $E$ is the modulus of elasticity of the rock formation; $m$ is the thickness of the rock formation, m.

Based on the amount of subsidence deformation of adjacent rock layers within the inter-layer rock, a flow chart is proposed to discern the formation index of fractures and determine the occurrence of separations. This flow chart is based on the modulus of elasticity $E$ of the rock layer and the thickness $m$ of the rock layer, as shown in Fig. 16. When the tensile stresses generated by the bending and sinking of the rock within the inter-layer meet the conditions for separation, and the deflection of the lower rock layer is greater than the upper rock layer, the adjacent upper and lower rock layers will create a separated, resulting in the formation of a horizontal separation fracture, $\omega_{max\ lower} > \omega_{max\ upper}$. Usually the span of the upper rock layer is approximately 0.8 times the span of the lower rock layer, $L_{upper} = L_{lower}$. Conversely, when the lower rock deflection is less than the upper rock deflection, $\omega_{max\ lower} = \omega_{max\ upper}$, there will be simultaneous bending subsidence without transverse separation fractures, usually the span of the upper rock layer is the same as the span of the lower rock layer, $L_{upper} = L_{lower}$.

Determination of the amount of off-layer for tension off-layer fractures. According to the masonry beam mechanics model, the sinking curve of the rock beam in layer $i$ of the inter-layer rocks can be expressed by the following Eq. (37):

$$W_{xi} = \left[ m - \sum h_i' \left( K_{pi}' - 1 \right) \right] \left( 1 - e^{-\frac{x}{2l_i}} \right) \tag{37}$$

$$l_i = h_i \sqrt{\frac{R_T}{3q}} \tag{38}$$

where $W_{xi}$ is the sinking curve of the $i$ rock layer within the inter-layer at $x$ m from the coal wall of the working face; $K_{pi}'$ is the residual fragmentation and expansion coefficient of the $i$ rock layer within the inter-layer; $\sum h_i'$ is the distance between the $i$ rock beam and the coal seam of the inter-layer, m; $l_i$ is the fracture distance of the $i$ rock layer, m; $h_i$ is the thickness of the $i$ rock layer, m; $R_T$ is the tensile strength of the $i$ rock layer; $q$ is the load of the overlying rock layer of the $i$ rock layer, $kN/m^3$.

The amount of subsidence after the $i$ rock formation has been stabilized by subsidence is

$$W_{mi} = m - \sum h_i' \left( K_{pi}' - 1 \right) \tag{39}$$

After the two adjacent rock layers of the inter-layer have sunk and stabilized, the maximum amount of separation before breakage occurs is:

$$\Delta W_{mi} = W_{mi} - W_{mi+1} = \sum h_{i+1}' \left( K_{pi+1}' - 1 \right) - \sum h_i' \left( K_{pi}' - 1 \right) \tag{40}$$
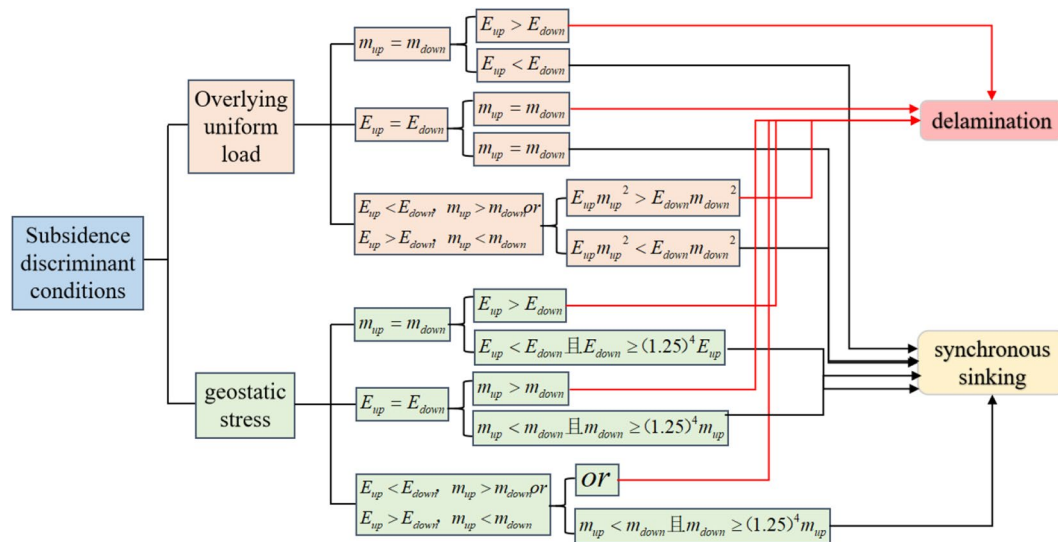
**Fig. 16** Flow chart for determining the formation of horizontal separation fracture

The amount of separation after the breaking of the two adjacent rock layers is:

$$\Delta W_{mi} = W_{mi}\left(e^{-\frac{x}{2l_{i+1}}} - e^{-\frac{x}{2l_i}}\right) \tag{41}$$

According to the theory of thin plates in elastic mechanics, the amount of separation of adjacent rock layers can be expressed as follows:

$$\Delta W_{max} = \frac{a_1^4}{\pi^4\left[3 + 3\left(\frac{a_1}{b_1}\right)^4 + 2\left(\frac{a_1}{b_1}\right)^2\right]}\left(\frac{q_{lower}}{D_{lower}} - \frac{q_{upper}}{D_{upper}}\right) \tag{42}$$

where $\Delta W_{max}$ is the maximum separation of the adjacent rock sheet; $a_1$ is the length of the rock sheet; $b_1$ is the width of the rock sheet; $q_{upper}$ and $q_{lower}$ are the mean load of the adjacent upper and lower rock sheets, respectively; $D_{upper}$ and $D_{lower}$ are the bending stiffness of the adjacent upper and lower rock sheets, respectively.

2. Horizontal shears staggered fractures

In the process of mining the lower group coal seams, adjacent rock layers with large differences in bending stiffness are prone to separation. Adjacent rock layers without separation will have synchronized bending and subsidence deformation to form horizontal shear staggered fractures. It is regarded as a combined rock beam model. The transverse separation fracture serves as the boundary of the combined rock beam, as shown in Fig. 17a. In the process of inter-layer rock mining and sinking, let $i \sim j$ represent the unit width of the combined rock beam model. Since the bending radius

of curvature of the inter-layer rocks is much larger than the thickness of the rock layer, we take the radius of curvature of each rock layer on the combined rock beam model as the radius of curvature of the lower most rock layer. A right angle coordinates system is established with the neutral rock layer of the combined beam as the $x - y$ plane. The bending moment of the combined rock beam model is the sum of the bending moments of each rock layer in any longitudinal section. This can be expressed as shown in Eq. (43).
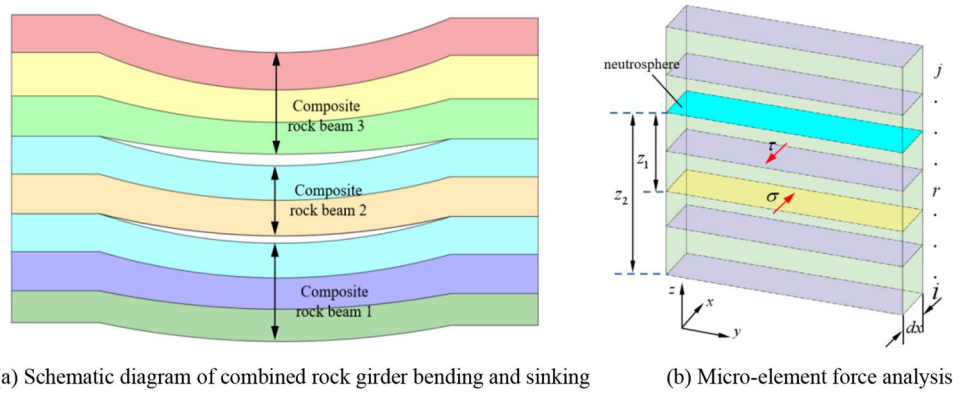
$$\overline{M}_{i\sim j} = \sum_{n=i}^{j} M_n = \sum_{n=i}^{j}\left(\int_{h_n} \sigma_n z dz\right) = \sum_{n=i}^{j}\left(\frac{E_n}{\overline{\rho}_{i\sim j}}\int_{h_n} z^2 dz\right) = \frac{1}{\rho_i}\sum_{n=i}^{j} E_n I_n \tag{43}$$

where $\overline{M}_{i\sim j}$ is the equivalent bending moment of the combined rock beam between the layers, $kN \cdot m^3$; $M_n$ is the bending moment of the $n$ rock layer, $kN \cdot m$; $h_n$ is the thickness of the $n$ rock layer, $m$; $\sigma_n$ is the positive stress in the longitudinal section of the $n$ rock layer, $MPa$; $\overline{\rho}_{i\sim j}$ is the equivalent radius of curvature of the combined rock beam, $m$; and $\rho_i$ is the radius of curvature of the $i$ rock layer, $m$. From Eq. (43), it follows that:

$$\frac{E_i I_i}{M_i} = \rho_i = \frac{\sum_{n=i}^{j} E_n I_n}{\overline{M}_{i\sim j}} \tag{44}$$

The simultaneous bending deformation of the layers of the combined rock beam within the inter-layer rock shows that the positive strain in the horizontal direction at any point along the longitudinal section is only related to the longitudinal coordinate. The modulus of elasticity is related to the

**Fig. 17** Modeling of shear staggered fractures in rock beams of inter-layer rock



(a) Schematic diagram of combined rock girder bending and sinking　　　　(b) Micro-element force analysis

lithology of the inter-layer. Therefore, the positive stress at a point with a longitudinal coordinate $z$ on the longitudinal section of the longitudinal section of the $r$ rock layer of the combined rock beam is:

$$\sigma_r = \frac{E_r Z}{\rho_i} = \frac{\overline{M}_{i\sim j} E_r Z}{\sum\limits_{n=i}^{j} E_n I_n} \quad (i \leq r \leq j) \tag{45}$$

A micro-element of length is taken inside the inter-layer composite rock beam $dx$. A cross-section is taken inside the micro-element, which is assumed to be located on the $r$ rocks layer and at a distance $h_r'$ from its lower surface. A spatial coordinate system is established in the plane where the neutral layer are located $x - y$. The vertical distances from the cross-section and the base of the micro-element from the neutral layer of the combined rock beam is $z_1$ and $z_2$ respectively, as shown in Fig. 17b.

Assuming that the tangential stress in the cross-section is $\tau_r$, the combined force in the direction $x$ below the cross-section is zero, which gives:

$$\tau_r dx - \int_{z_2}^{z_1} d\sigma dz = 0 \tag{46}$$

Substituting Eq. (45) into Eq. (46) and giving $dM/dx = Q$, which gives:

$$\tau_r = \frac{\overline{Q}_{i\sim j}}{\sum\limits_{n=i}^{j} E_n I_n} \left( \sum_{m=i}^{r-1} E_m \int_{h_m} z dz + E_r \int_{h_r'} z dz \right) = \frac{\overline{Q}_{i\sim j}}{\sum\limits_{n=i}^{j} E_n I_n} \left( \sum_{m=i}^{r-1} E_m h_m z_{cm} + E_r h_r' z_{cr}' \right) \tag{47}$$

where $z_{cm}$ are the longitudinal coordinating of the longitudinal section form center of rock layer $m$; $z_{cr}'$ is the longitudinal coordinate of the longitudinal section form center of the part of rock layer $r$ below the transverse section; $\overline{Q}_{i\sim j}$ is the equivalent shear force of the rock beam of the combination of the layers, $kN$. The equivalent shear force according to Eq. (44) can be expressed as shown in Eq. (48):

$$\overline{Q}_{i\sim j} = \frac{d\overline{M}_{i\sim j}}{dx} = \frac{\sum\limits_{n=i}^{j} E_n I_n}{E_i I_i} \frac{dM_i}{dx} = \frac{\sum\limits_{n=i}^{j} E_n I_n}{E_i I_i} Q_i \tag{48}$$

The above equations are based on the plane in which the neutral layer of the rock beam of the inter-layered rock combination is located, as a right-angle coordinates system $x - y$. If the plane in which the lower surface of the coal seam is located $x - y$ is a right-angle coordinate system and is substituted for Eq. (48), then Eq. (47) can be expressed as follows:

$$\tau_r = \frac{Q_i}{E_i I_i} \left[ \sum_{m=i}^{r-1} E_m h_m \left( H_m - h_m/2 - H_{neu} \right) + E_r h_r' \left( H_r - h_r'/2 - H_{neu} \right) \right] \tag{49}$$

where $H_{neu}$ is the vertical distance of the neutral rock seam from the lower surface of the coal seam, $m$. The $H_{neu}$ is obtained by taking the combined force in the horizontal direction to zero in any longitudinal section of the combined rock beam of the inter-layered rock.

From this, the vertical distance $H_{neu}$ from the neutral surface to the lower surface of the coal seam can be found as follows:

$$H_{neu} = \frac{\sum\limits_{n=i}^{j} E_n h_n \left( H_n - h_n/2 \right)}{\sum\limits_{n=i}^{j} E_n h_n} \tag{50}$$

Substituting Eq. (50) into Eq. (49) gives the shear stress in any cross-section of the combined rock beam from the $i \sim j$ rock formation. If this cross-section lies on the upper surface of the $r$ rock formation, $h_r' = h_r$, then Eq. (49) can be simplified to:

$$\tau_r = \frac{Q_i}{E_i I_i} \sum_{m=i}^{r} E_m h_m \left( H_m - h_m/2 - H_{neu} \right) \tag{51}$$

The shear strength of the upper surface of rock formation $r$, the contact surface between rock formation $r$ and rock formation $r + 1$, can be calculated according to the following equation:

$$\left[\tau_r^{in}\right] = \sum_{n=r+1}^{s} \gamma_n h_n \tan \phi_r^{in} + c_r^{in} \tag{52}$$

where $\left[\tau_r^{in}\right]$ is the shear strength on the adjacent rock contact surface, $MPa$; $\phi_r^{in}$ is the angle of internal friction on the adjacent contact surface, °; $c_r^{in}$ the cohesive force on the adjacent rock contact surface, $MPa$; When the horizontal stress formed on the contact surface by the bending and sinking of the combined rock beam is greater than its shear strength, shear damage occurs on the adjacent rock contact surface, producing horizontal shear staggered fractures.

The distribution characteristics of shear stress on the contact surface of a rock formation are the same as those of shear stress, with the shear stress on the contact surface gradually decreasing as one moves deeper into the formation. Horizontal shears staggered fractures are formed by the simultaneous bending deformation of the combined rock layers, resulting in horizontal shears stresses and shear damage to the contact surface. Shear staggered fractures exhibit slight tangential shear displacement along the fracture face and no displacement normal to the fracture face. As a result, Horizontal shear staggered fractures were formed.

3. Longitudinal tension fractures

During the mining process of the lower group of coal seams, the development and evolution of longitudinal tension fractures in the inter-layer rock is shown in Fig. 18.

The subsidence, bending moment, and radius of curvature of any $i$ formation within the inter-layer satisfy the following relationship:

$$\rho_i = \frac{E_i I_i}{M_i} = \frac{\left[1 + \left(\frac{dw_i}{dx}\right)^2\right]^{3/2}}{\frac{d^2 w_i}{dx^2}} \tag{53}$$

Since $\left(dw_i / dx\right)^2$ in Eq. (53) is much less than 1, it is calculated here as zero, so Eq. (53) can be reduced to (Liu 2011):

$$\rho_i = \frac{E_i I_i}{M_i} = 1 \bigg/ \frac{d^2 w_i}{dx^2} \tag{54}$$

According to the provisions of the mechanics of materials, it can be seen that when the rock layer bends upward the lower surface is tensile and the upper surface is compressive, and its bending moment and curvature are positive.

Assuming the maximum bending moment of rock formation $i$ is positive, its maximum tensile stress is located at the lower surface of the formation, which can be expressed as:

$$\left(\sigma_i^t\right)_{max} = \frac{E_i h_i}{2\rho_i} \tag{55}$$

By comparing the maximum tensile stress on the rock layer with the tensile strength of the rock layer itself, it can be analyzed that when the maximum tensile stress is greater than the tensile strength of the rock layer, the surface of the rock layer will produce tension fractures, and when the tensile stress at the tip of the fracture is equal to the tensile strength of the rock layer, the tension fractures will stop developing. It is assumed that tension fractures are generated on the lower surface of the $i$ rock formation, and the development of fractures stops when the crack development length is $l_i^f$. Since the development length of the fracture is much smaller than the radius of curvature of the rock layer, it is assumed that the radius of curvature does not change before and after the development of the fracture, and the tensile stress at the tip of the crack on the lower surface of the intact rock layer can be obtained as:

$$\left(\sigma_i^t\right)'_{max} = \frac{E_i \left(h_i - l_i^f\right)}{2\rho_i} \tag{56}$$

The maximum tensile stress at the tip is equal to the tensile strength of the rock formation, then

$$\left[\sigma_i^t\right] = \left(\sigma_i^t\right)'_{max} \tag{57}$$

Combining Eqs. (56) and (57) gives the development length of tension fractures as:

$$l_i^f = h_i - \frac{2\rho_i \left[\sigma_i^t\right]}{E_i} \tag{58}$$

4. Longitudinal shear fractures

The formation of longitudinal shear fractures in interlayer rock is typically the result of the combined action of tensile and shear forces. These fractures occur when the maximum bending tensile stress at the surface of the formation exceeds the tensile strength of the rock. As the fractures develop along the surface of the formation, their length increases and the tensile stress at the fracture tip decreases. Eventually, when the tensile stress becomes lower than the tensile strength of the rock formation, the development of the tension fractures stops. The development of tension fractures reduces the effective bearing section of the rock formation on the fracture face. However, under the condition that the shear force remains unchanged, the shear stress
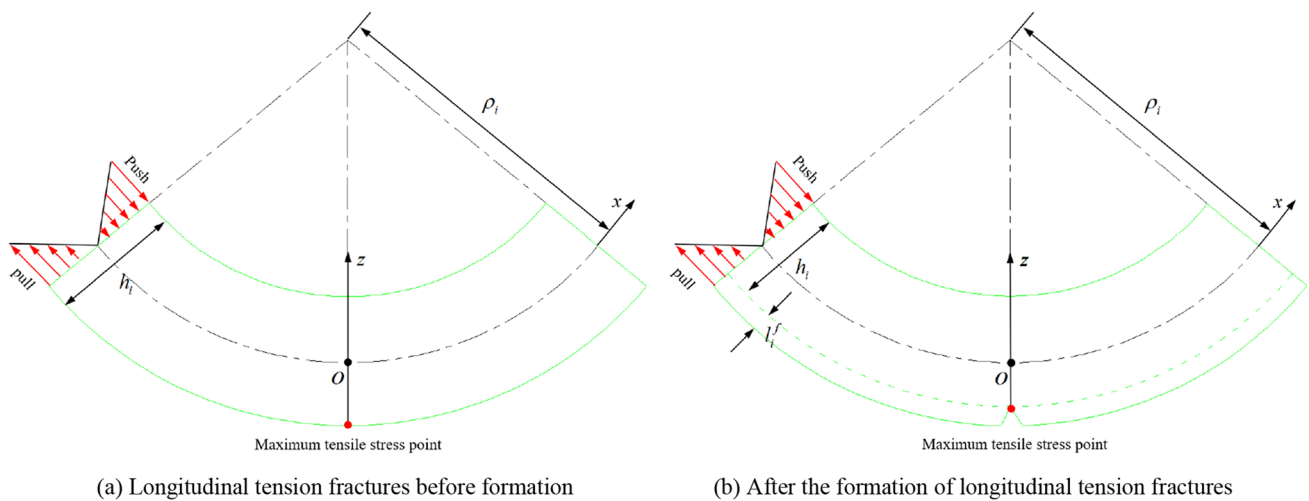
(a) Longitudinal tension fractures before formation

(b) After the formation of longitudinal tension fractures

**Fig. 18** The development process of longitudinal tensile fractures in rock strata

in the section increases. This combined action of tension and shear forces leads to the formation and development of longitudinal shear fractures in the inter-layered rock. When the shear stress exceeds the shear strength of the formation, the fracture will continues to develop until it penetrates the formation. This results in the formation shears off along the fracture face (Liu 2011), creating a longitudinal shear fracture. In the entire inter-layer rock, the distribution of shear stress in its longitudinal section is characterized by higher values on both sides and lower values in the middle. The maximum shear stress is distributed on the neutral layer as follows:

$$(\tau_i)_{\max} = \frac{3Q_i}{2h_i} \tag{59}$$

When the longitudinal shear fractures development length of the rock formation is $l_i^f$, assuming that the shear force acting on the section of the formation remains $Q_i$, the maximum shear stress is:

$$(\tau_i)'_{\max} = \frac{3Q_i}{2\left(h_i - l_i^f\right)} \tag{60}$$

The formation of longitudinal shear fractures within the inter-layer rock depends primarily on the maximum shear stress and the shear strength of the rock itself. When the maximum shear stress exceeds the shear strength of the rock layer, the rock layer will shear along the surface of the fractures, resulting in the penetration of longitudinal shear fractures. The aforementioned longitudinal shear fractures mainly apply to a single rock layer. In case where there are multiple layers with simultaneous bending deformation, it is possible considered a combined rock beam model for

analysis. The positive and shear stresses in the longitudinal section of the combined rock beam can be calculated using Eqs. (45) and (49) mentioned above. These calculations can help determine the length of the longitudinal shear fracture development in the combined rock beam.

Based on the above analysis, the formation of fractures in the inter-layered rock is primarily influenced by the combination of different coal mining methods used for the upper group of coal seams and the lower group of coal seams. This combination leads to the development of macroscopic and microscopic fractures in the inter-layered rock. These fractures are formed due to the combined effect of horizontal tension off-layer fractures, horizontal shears staggered fractures, longitudinal tension fractures, and longitudinal shear fractures. When the upper group of coal seams is mined using long-wall fully mechanized coal mining, the dominant formation of inter-layer rock fractures is characterized by horizontal shear staggered fractures and longitudinal tension fractures. On the other hand, when the upper group of coal seams is mined using room-and-pillar mining, the dominant formation of inter-layer rock fractures is characterized by longitudinal tension fractures and longitudinal shear fractures. Similarly, when the lower group of coal seams is mined using long-wall fully mechanized coal mining, the dominant formation of inter-layered rock fractures includes horizontal tension fractures, longitudinal tension fractures, and longitudinal shear fractures. As the mining area passes through the the fully mechanized mining area, horizontal tension fractures, and longitudinal shear fractures become dominant. Conversely, when passing through the room-and-pillar mining area, longitudinal tension fractures and longitudinal shear fractures are dominated. Therefore, the formation of the inter-layer rocks fracture system is

a result of the combined effect of transverse separation fractures and longitudinal breaking fractures.

# 5 Conclusion

1. During the mining process of the upper and lower coal seams, there is a gradual increase in the density and width of fractures in the inter-layered rock. These fractures primarily included lateral boundary breaking fractures, transverse separation fractures, and longitudinal breaking fractures. The overall distribution of fracture evolution in the inter-layered rock exhibits a positive trapezoidal pattern. In the inter-layer rock below the fully mechanized mining area, the longitudinal breaking fractures exhibits a similar breakage distance as the key rock layers, displaying noticeable periodicity. The development of inter-layer rock fractures on the open-off cut side and the mining side of the working face is significantly greater compared to the fractures in the middle part of the inter-layered rock. The development of longitudinal breaking fractures and lateral boundary breaking fractures in the inter-layered rock below the room-and-pillar mining area does not exhibit significantly periodic. However, the fracture width and density in this area are significantly compared to those in the inter-layered rock below the fully mechanized mining area. In addition, the development of longitudinal breaking fractures is less correlated with the breakage of key rock layers.

2. The stress distribution of the inter-layered rock under the fully mechanized mining area exhibits distinct regions, namely the compression region, transition region, expansion region, and re-compaction region. In contrast, the stress distribution of the inter-layered rock under the room-and-pillar mining area is limited to the compression region and expansion region. Based on the characteristics of the stress distribution in the inter-layered rock, a stress fracture expansion model is developed to explain the fracture development in different stress regions. This model helps determine the mechanism of fracture development in the inter-layered rocks under different mining areas of the upper group coal seam.

3. The development of inter-layer rock fractures is primarily influenced by the different coal mining methods used for the upper group coal seams and the lower group coal seams. The formation of macroscopic and microscopic fractures in the inter-layer rock is a result of the combined effect of horizontal tension off-layer fractures, horizontal shear staggered fractures, longitudinal tension fractures, and longitudinal shear fractures. When the lower group coal seam passes through the fully mechanized mining area, the inter-layered rock fractures are mainly characterized by horizontal tension off-layer fractures and longitudinal shear fractures. On the other hand, when it passes through the room-and-mining area, the dominant fractures are longitudinal tension fractures and longitudinal shear fractures.

# References

Aben FM, Doan ML, Mitchell TM, Toussaint R, Reusché T, Fondriest M, Gratier JP, Renard F (2016) Dynamic fracturing by successive coseismic loadings leads to pulverization in active fault zones. J Geophys Res Solid Earth 121(4):2338–2360

Bai Q, Tu S (2020) Numerical observations of the failure of a laminated and jointed roof and the effective of different support schemes: a case study. Environ Earth Sci 79(10):202

Bai QS, Tu SH, Zhang C, Zhu D (2016) Discrete element modeling of progressive failure in a wide coal roadway from water-rich roofs. Int J Coal Geol 167:215–229

Basista M, Gross D (1998) The sliding crack model of brittle deformation:an internal variable approach. In J Solids Struct 35(5–6):487–509

Cai JJ, Li XJ, Guo LX, Xue HT, Xu BZ (2022) Fracture development and multifield coupling evolution law of soft overburden rock in a medium-thick coal seam mine. Geofluids 2022:1–14

Feng GR, Wang SW, Guo YX, Zhang YJ, Bai JW, Du YL (2021) Optimum position of roadway in the middle residual coal seam between the upper and lower longwall gobs. Energy Sources Part A Recov Util Environ Eff. https://doi.org/10.1080/15567036.2021.1897709

Gong H, Luo Y, Zhou J, Zhao CC, Li XP (2023) Fracture behaviors and damage evolution anisotropy of granite under coupling of multiaxial confinement and dynamic loading. Rock Mech Rock Eng 56:2515–2534

He CC, Lu WY, Zha WH (2020) Evolution mechanism of inter-connected vertical fractures in the overburden of longwall coal mining. Geofluids 2020:1–12

Huang QX, Han JB (2019) Study on fracture evolution mechanism of shallow-buried close coal seam mining. J Min Saf Eng 36(04):706–711

Huang QH, He YP, Luo LB, Cao J (2018) Study on the active structure of caved roof and support resistance in shallow buried and ultra-close coal seams mining. J Min Saf Eng 35(03):561–566

Huang QX, Zhao MY, Huang KJ (2019) Study of roof double key strata structure and support resistance of shallow coal seams group mining. J China Univ Min Technol 48(01):71–77+86

Liu HW (2011) Mechanics of materials. Higher Education Press, Beijing

Liu C, Li X, Zhang C, Sun BQ (2021) The spatio-temporal evolution law of overlying rock fractures in an experimental working face (N00 mining method) based on microseismic monitoring technology. Arab J Geosci 14:1373

Lu W, He C, Zhang X (2020) Height of overburden fracture based on key strata theory in longwall face. PLoS ONE 15(1):e0228264

Song Y, Yang SQ, Li KS, Yin PF, Pan PZ (2023) Mechanical behavior and fracture evolution mechanism of composite rock under triaxial compression: insights from three-dimensional DEM modeling. Rock Mech Rock Eng 56:7673–7699

Wang XL (2022) Similar simulation test of overlying rock failure and crack evolution in fully mechanized caving face with compound roof. Geotech Geol Eng 40:73–82

Wang XY, Song XM, Chen CH (2016) The impact study on strata behavior laws of different coal seam spacing in ultra closed coal seams. J Min Saf Eng 33(01):116–121

Wang Y, Tan WH, Liu DQ, Li CH (2019) On anisotropic fracture evolution and energy mechanism during marble failure under uniaxial deformation. Rock Mech Rock Eng 52:3567–3583

Wang Y, Feng WK, Hu RL, Li CH (2021) Fracture evolution and energy characteristics during marble failure under triaxial fatigue cyclic and confining pressure unloading (FC-CPU) conditions. Rock Mech Rock Eng 54:799–818

Xu MT, Xu YL, Jin ZY (2020) Research on support resistance of contiguous coal seam mining under room-and-pillar gob. Coal Sci Technol 48(08):63–69

Yang GS, Wang JS (2018) Overburden structure evolution and pressure law of second mining in close-range coal seam group. J China Coal Soc 43(S2):353–358

Yu MG, Teng F, Chu TX, Chao JK, Li P (2018) Simulation study on the evolution of overlying strata fracture development and air-leaking passage under repeated coal-mining of shallow buried coal seams. J Henan Polytech Univ 37(1):001–007

Zhang Y, Zhang CL, Zhao F (2015) Dynamic evolution rules of mining-induced fractures in different floor area of short-distance coal seams. J China Coal Soc 40(4):786–792

Zhang J, Yang T, Wang B, Zhang Q, Liu D, Reng YB (2017) Prediction analysis of mining roof water-inrush in shallow coal seams with surface valley run off. J Min Saf Eng 34(05):868–875

Zhang ZX, Zhang YB, Xu YX, Zheng Q, Wang ZL, Guo LL (2021) Fracture development and fractal characteristics of overburden rock under repeated mining. Arab J Geosci 14:225

Zhou XP, Zhang YX (2007) Constitutive theory and application of unloading rock mass. Science Press, Beijing, pp 55–72

Zhou XP, Ha QL, Zhang YX (2005) Analysis of local-ization of formation and complete stress-strain relation for mesoscopic heterogeneous brittle rock materials when axial stress is held constant while lateral confinement is reduced. Chin J Rock Mech Eng 24(18):3236–3245

Zhu DF (2018) Study on the bearing characteristics of shallow non-sufficient collapse mining area and the mechanism of disaster caused by repeated mining. Dissertation, China University of Mining and Technology

Zhu DF, Tu SH, Tu HS, Li XY, Liang NG (2018) Analysis of stress propagation mechanism in the interval coal pillars under the gully landform. J Min Saf Eng 35(04):701–707

Zhu WB, Xu JL, Chen Lu, Li Z, Liu WT (2019) Mechanism of disaster induced by dynamic instability of coal pillar group in room-and-pillar mining of shallow and close coal seams. J China Coal Soc 44(2):358–366

Zhu HQ, Fang SH, Huo YJ, Guo JL, Wu Y, Hu LT (2020) Study of the dynamic development law of overburden breakage on mining faces. Sci Rep 10:6555